Draft 07.02.14_upd

Letter of Intent.

Nec sine te, nec tecum vivere possum. (Ovid)*

Spin Physics Experiments at NICA-SPD with polarized proton and deuteron beams.

(Updating list of participants)
F. Ahmadov[1], R.R. Akhunzyanov[1], V. A. Anosov[1], N.V. Anfimov[1], S. Anishchanka[12], X. Artru[15], A.A.Baldin[1], V.G. Baryshevsky[12], A. S. Belov[5], D. A. Bliznyuk[14], M.Bodlak[8], A.V. Butenko[1], A. P. Cheplakov[1], I. E. Chirikov-Zorin[1], G. Domanski[10], S.V. Donskov[6], M. Dziewiecki[10], A.V. Efremov[1], Yu. N. Filatov[1,3], V.V. Fimushkin[1], M. Finger (jun.)[7,1], M. Finger[7,1], S.G. Gerassimov[13], I.A. Golutvin[1], B.V. Grinyov[14], A. Gurinovich[12], A.V. Guskov[1], Yu. I. Ivanshin[1], A.V. Ivanov[1], V. Jary[8], A. Janata[7,1], N. Javadov[1], L. L. Jenkovszky[4], V. D. Kekelidze[1], A.P. Kobushkin[4], B. Konarzewski[10], A. M. Kondratenko[2], M. A. Kondratenko[2], I. Konorov[13], A. D. Kovalenko[1], O. M. Kouznetsov[1], G. A. Kozlov[1], Z.V. Krumshtein[1], V.V. Kukhtin[1], K. Kurek[9], P. K. Kurilkin[1], R. Kurjata[10], L.V. Kutuzova[1], V. P. Ladygin[1], R. Lednicky[1], A. Lobko[12], A.I. Malakhov[1], J. Marzec[10], J. Matousek[7], G.V. Meshcheryakov[1], V. A. Mikhaylov[1], Yu.V. Mikhaylov[6], P.V.Moissenz[1], V.V.Myalkovskiy[1], A. P. Nagaytsev[1], J. Novy[8], I.A.Orlov[1], M. Pesek[7], D.V. Peshekhonov[1], V. D. Peshekhonov[1], V. A. Polyakov[6], Yu.V. Prokofichev[1], V. K. Rodionov[1], N. S. Rossiyskaya[1], A. Rouba[12], A. Rychter[10], V. D. Samoylenko[6], A.Sandacz[9], I. A. Savin[1], O.Yu. Shevchenko[1], S.S. Shimanskiy[1], M. Slunechka[7,1], V. Slunechkova[7,1], J. Soffer[11], G.I.Smirnov[1], N. B. Skachkov[1], E. A.Strokovsky[1], O.V.Teryaev[1], M. Tomasek[8], N.D.Topilin[1], A.V.Turbabin[5], M.Virius[8], V.Vrba[8], M.V. Zavertyaev[13], K. Zaremba[10], E.V. Zemlyanichkina[1], P.N. Zhmurin[14], M. Ziembicki[10], V. N. Zubets[5], I.P. Yudin[1]

---

*Neither without you, nor with you one can live.

[15]CNRS, Lion, France
[14]Institute for Scintillation Materials, NAS, Kharkov, Ukraine
[13]Lebedev Physics Institute, Moscow, Russia
[12]Research Institute for Nuclear Problems, Minsk, Belarus
[11]Temple University, Philadelphia, USA
[10]Warsaw University of Technology, Institute of Radio electronics, Warsaw, Poland
[9]National Center for Nuclear Research, Warsaw, Poland
[8]Technical University, Faculty of Nuclear Science and Physics Engineering, Prague, Czech Rep.
[7]Charles University, Faculty of Mathematics and Physics, Prague, Czech Republic
[6]Institute for High Energy Physics, Protvino, Russia
[5]Institute for Nuclear Research of Russian Academy of Sciences, Moscow, Russia
[4]Bogolyubov Institute for Theoretical Physics, Kiev, Ukraine
[3]Moscow Institute of Physics and Technology, Dolgoprudny, Russia
[2]Science and Technique Laboratory Zaryad, Novosibirsk, Russia
[1]Joint Institute for Nuclear Research, Dubna, Russia

TABLE OF CONTENTS

1. Introduction. (IS)*) ……………………………………………………………..3
1.1. Basic PDFs of nucleons.
1.2. DIS as a microscope for nucleons. The PDF f_1 and g_1.
1.3. New TMD PDFs.
1.4. Other actual problems of high energy physics.
2. Physics motivations. ……………………………………………………………..12
2.1. Nucleon spin structure studies using the Drell-Yan (*DY*) mechanism. (AE)
2.2. New nucleon PDFs and J/Ψ production mechanisms. (OSh)
2.3. Direct photons. (AG)
2.4. Spin-dependent high-p_T reactions. (SSh)
2.5. Spin-dependent effects in elastic *pp* and *dd* scattering. (OT)
2.6. Spin-dependent reactions in heavy ion collisions. (OT)
2.7. Future experiments on nucleon structure in the world. (AN)
3. Requirements to the NUCLOTRON-NICA complex. (IS)…………………………25
4. Polarized beams at NICA. (ADK) ……………………………………………………25
4.1. Scheme of the complex.
4.2. Source of polarized ions (SPI).
4.3. Acceleration of polarized ions at Nuclotron.
4.4. NICA in the polarized proton and deuteron modes.
4.5. Polarimetry at SPI, Nuclotron and NICA.
5. Requirements to the spin physics detector (SPD). (AN, IS) ………………………...31
5.1. Event topologies.
5.2. Possible layout of SPD.
5.3. Trigger system.
5.4. Local polarimeters and luminosity monitors.
5.5. Engineering infrastructure.
5.6. DAQ.
5.7 SPD reconstruction software.
5.8 Monte Carlo simulations.
5.9. Slow control.
5.10. Data accumulation, storing and distribution.
6. Proposed measurements with SPD. ……………………………………………….40
6.1. Estimations of *DY* and J/Ψ production rates. (AN, OSh)
6.2. Estimations of direct photon production rates. (AG)
6.3. Rates in high-p_T reactions. (SSh)
6.4. Rates in elastic *pp* and *dd* scattering.
6.5. Feasibility of the spin-dependent reaction studies in heavy ion collisions.
7. Time lines of experiments. ……………………………………………………….44
8. References. ………………………………………………………………………. 45

---

*) (..) Convener(s) of the Section

1. Introduction

Main parts of this Letter of Intent (LoI) are related to the studies of the nucleon structure. The beginning of the nucleon structure story refers to the early 50-ties of the 20th century when in the famous Hofstadter's experiments at SLAC the proton electromagnetic form factor was measured determining thus the proton radius of $\langle r_p \rangle = (0.74 \pm 0.24) \cdot 10^{-13}$ cm. It means that the proton is not an elementary particle but the object with an internal structure. Later on, again at SLAC, the point-like ***constituents*** have been discovered in the proton and called ***partons***. After some time, in 1970-ties, partons were identified with ***quarks*** suggested early by Gell-Mann as structure-less constituents of all hadrons. Three families of quarks, each containing two quarks and anti-quarks, are now the basic elements of the Standard Model (SM) of elementary particle structure. All six quarks are discovered.

The naïve quark-parton model (***QPM***) of nucleons, i.e. of the proton and neutron, has been born. According to this model, the proton (neutron) consisted of three spin1/2 ***valence quarks***: two (one) of the ***u***-type and one (two) of the ***d***-type with a charge of (+2/3) e and (-1/3) e, respectively, where e is the charge of the electron. Quarks interact between themselves by ***gluon*** exchange. Gluons are also the nucleons constituents. Gluons can produce a ***sea*** of any type (***flavor***) quark-antiquark pairs. Partons share between themselves fractions, x, of the total nucleon momentum. Parton Distribution Functions (***PDFs***) are universal characteristics of the internal nucleon structure.

Now the quark-parton structure of nucleons and respectively the quark-parton model of nucleons are becoming more and more complicated. In Quantum Chromo Dynamics (QCD), PDFs depend not only on x, but also on Q^2, four-momentum transfer (see below). Partons can have an internal momentum, k. A number of PDFs depends on the order of the QCD approximations. Therefore, the measurements of new collinear and Transverse Momentum Dependent (TMD) PDFs, the most of which are not discovered yet, are proposed in this LoI. Main ideas of this document have been discussed at the specialized International Workshops [1]. General organization of the text follows the Table of contents.

1.1. Basic (twist-2) PDFs of the nucleon.

There are three PDF, integrated over the possible internal transverse momentum of parton, k_T, characterizing the nucleon structure at the leading QCD order (twist-2). These PDFs are: the distribution of parton ***density*** in non-polarized (U) nucleon, $f_1(x, Q^2)$; the distribution of longitudinal polarization of quarks in longitudinally polarized (L) nucleon (***helicity***), $g_1(x, Q^2)$; and the distribution of transverse polarization of quarks in transversely polarized (T) nucleon (***transversity***), $h_1(x, Q^2)$. They are shown as diagonal terms in Fig.1.1 with the nucleon polarization (U, L, T) along the vertical direction and the quark polarization along the horizontal direction. The PDF $h_1(x, Q^2)$ is poorly studied. It is a chiral-odd function which can be measured in combination with another chiral-odd function. If one takes into account the possible transverse momentum of quarks, k_T, there will be five additional Transverse Momentum Dependent (TMD) PDFs which are functions of three variables: x, k_T, Q^2. These TMD PDFs are: correlation between the transverse polarization of nucleon (transverse spin) and the transverse momentum of non-polarized quarks (***Sivers***), $f^{\perp}_{1T}$; correlation between the transverse spin and the longitudinal quark polarization (***worm-gear-T***), $g^{\perp}_{1T}$; distribution of the quark transverse momentum in the non-polarized nucleon (***Boer-Mulders***), $h^{\perp}_{1}$; correlation between the longitudinal polarization of the nucleon (longitudinal spin) and the transverse momentum of quarks (***worm-gear-L***), $h^{\perp}_{1L}$; distribution of the transverse momentum of quarks in the transversely polarized nucleon (***pretzelosity***), $h^{\perp}_{1T}$. All new PDFs, except $f^{\perp}_{1T}$, are chiral-odd. The Sivers and Boer-Mulders PDFs are T-odd ones. At the sub-leading twist (twist-3), there are still 16 TMD PDFs containing the information on the nucleon structure. They have no definite physics interpretation. The PDFs

f_1 and g_1 are measured rather well (Section 1.2). The h_1 has been measured recently but is still poorly investigated. All TMD PDFs are currently studied (Section 1.3).

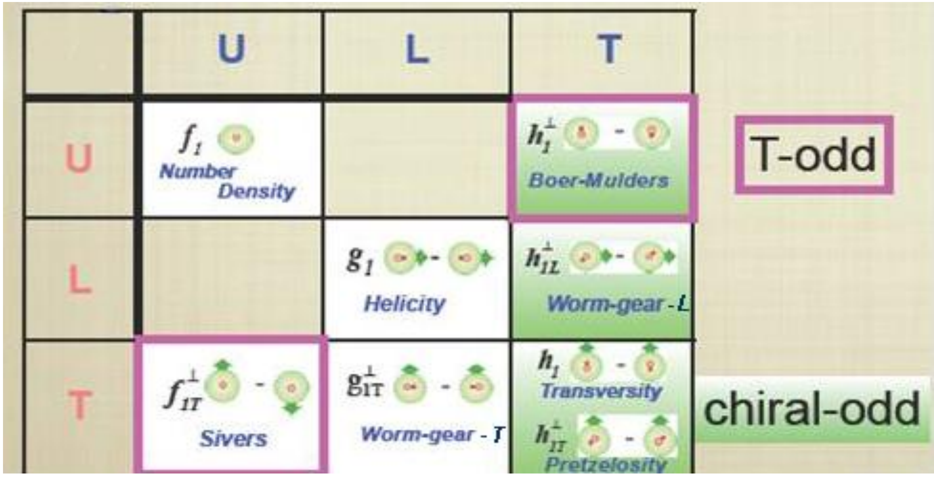

Fig.1.1*: the twist-2 PDFs characterizing the nucleon structure.*

1.2. Deep Inelastic Scattering as a microscope for the nucleon structure study. The PDF f_1 and g_1.

A powerful method to study the quark-parton structure of nucleons is the Deep Inelastic lepton-nucleon Scattering (DIS). High energy DIS of leptons off polarized nucleons also probes the polarization of quarks inside the polarized target and allows measuring the contribution of quarks to the spin of the nucleon. There are three types of DIS reactions:
- Inclusive (IDIS), when characteristics of incident (*l*), polarized or non-polarized, and scattered lepton (*l'*) are known (measured): $l + N \rightarrow l' + X$, nucleon *(N)* can be polarized or not;
- Semi-inclusive (SIDIS), when, additionally to the above mentioned, characteristics of one or more the final state hadron (*h*) are known: $l + N \rightarrow l' + nh + X$, n ≥1, and
- Exclusive (EDIS), initial and final states of the reaction are fully determined.

A quantitative characteristic of the IDIS reaction is a double differential cross section [2]. This cross section can be calculated theoretically assuming that the main contribution to it comes from the one-photon exchange process, represented by the Feynman diagram in Fig.1.2 (a). It is known that the one-photon exchange IDIS cross section is defined as

$$\vec{\sigma}_{one-photon} \equiv \frac{d^2\vec{\sigma}^{S_\ell S_N}}{d\Omega dE'} = \left(\frac{4\alpha^2}{Q^4}\cdot\frac{E'}{E}\right)\cdot L_{\mu\nu}\cdot W^{\mu\nu}.$$

The term in brackets characterizes the point-like interaction; $L_{\mu\nu}$ is the lepton current tensor representing the lepton vertex in Fig.1.2 (a) and $W^{\mu\nu}$ is the hadronic tensor amplitude characterizing the hadron vertex structure. Each tensor has two parts, one of which (SIM) is independent of the spin orientations and the second one (ASIM) is spin-dependent:

$$L_{\mu\nu} = L_{\mu\nu}^{SIM} + iL_{\mu\nu}^{ASIM},$$
$$W^{\mu\nu} = W_{SIM}^{\mu\nu} + iW_{ASIM}^{\mu\nu}.$$

The form of $L_{\mu\nu}$ is exactly known from Quantum ElectroDynamics (QED). The hadronic tensor $W^{\mu\nu}$ is not calculated theoretically. It is a pure phenomenological quantity characterizing the nucleon structure. Theory tells us that, from the most common considerations, for electromagnetic interactions $W^{\mu\nu}$ should have the form:

$$W^{\mu\nu}_{\rm SIM} = A^{\mu\nu}_1(q,q')\cdot W_1(Q^2,\nu) + A^{\mu\nu}_2(q,q')\cdot W_2(Q^2,\nu),$$
$$W^{\mu\nu}_{\rm ASIM} = B^{\mu\nu}_1(q,q')\cdot G_1(Q^2,\nu) + B^{\mu\nu}_2(q,q')\cdot G_2(Q^2,\nu),$$

where A_1, A_2, B_1 and B_2 are known kinematic expressions, $W_1(Q^2,\nu)$ and $W_2(Q^2,\nu)$ are spin independent and $G_1(Q^2,\nu)$ and $G_2(Q^2,\nu)$ are spin dependent structure functions representing the nucleon structure. In general, these structure functions should be functions of two independent variables - either (Q^2,ν); or (Q^2, x); or (x, y), etc. Bjorken has assumed that in the DIS (scaling) limit ($Q^2,\nu\rightarrow\infty$, x fixed), , the structure functions became the functions of the only one (Bjorken) scaling variable x:

$$M\cdot W_1(Q^2,\nu)\rightarrow F_1(x),$$
$$\nu\cdot W_2(Q^2,\nu)\rightarrow F_2(x),$$
$$\nu M^2\cdot G_1(Q^2,\nu)\rightarrow g_1(x),$$
$$\nu^2 M\cdot G_2(Q^2,\nu)\rightarrow g_2(x).$$

But at the Q^2 of current experiments, this hypothesis is true only in the limited range of x.

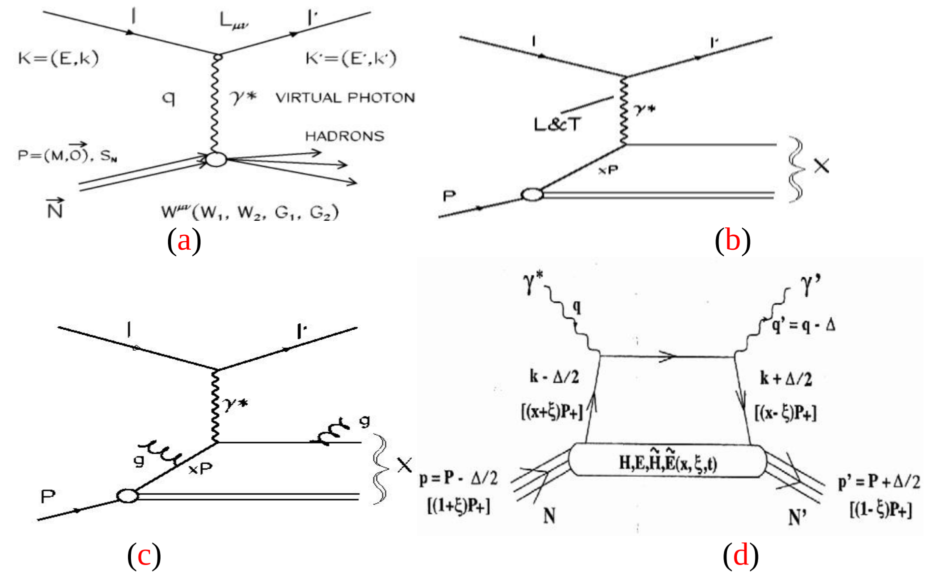

Fig.1.2: *Feynman diagrams of DIS in one-photon exchange approximation:*
(a) IDIS. The virtual photon transfers a four momentum squared, Q^2, and energy, ν, from the incident lepton to the nucleon. Variables: $-q^2 \equiv Q^2 = -(k-k')^2 = 4EE'\sin^2(\theta/2)$;

$$\nu = \frac{P\cdot Q}{M} = E - E'; \qquad x = Q^2/2M\nu; \qquad y = \nu/E$$

(b) IDIS in QPM. The virtual photon is absorbed by the constituent quark carrying the fraction of the nucleon momentum x;
(c) IDIS in QCD improved QPM. The quark absorbing the virtual photon can emit gluons before or after absorption;
(d) EDIS: the hand-bag diagram introducing Generalized Parton Distributions, GPD.

Performing the calculations as prescribed above and summing over the spin orientations of scattered leptons, S_e, which are usually not known, one can get the cross section

$$\frac{d^2\vec{\sigma}^{S_eS_N}}{d\Omega dE'} = \frac{d^2\sigma^{unp}}{d\Omega dE'} + S_N S_e \frac{d^2\sigma^{pol}}{d\Omega dE'},$$

where σ^{unp} (σ^{pol}) is the non-polarized (polarized) part of the cross section and $S_N = \pm 1$ is the orientation (helicity) of the nucleon spin. In the most commonly used notations the spin-independent part of the cross section, σ^{unp}, is expressed via two spin-independent structure functions F_1 and F_2:

$$\frac{d^2\sigma^{upn}}{dxdQ^2} = \frac{4\pi\alpha^2}{Q^2 x}\left[xy^2(1-\frac{2m_e^2}{Q^2})F_1(x,Q^2) + (1-y-\frac{\gamma^2 y^2}{4})F_2(x,Q^2)\right].$$

Here m_e is the lepton mass and $\gamma = 2Mx/\sqrt{Q^2} = \sqrt{Q^2}/\nu$. There is a theoretical relationship between the structure functions F_1 and F_2 known under the name of Callan-Gross:

$$F_2(x, Q^2) = 2xF_1(x, Q^2).$$

The σ^{unp} is often expressed via $F_2(x, Q^2)$ and $R(x, Q2) = \sigma_L/\sigma_T$ where $\sigma_L(\sigma_T)$ is the nucleon absorption cross section of the virtual photon with longitudinal (transverse) polarization:

$$\sigma^{unp} \equiv \frac{d^2\sigma^{unp}}{dxdQ^2} = \frac{4\pi\alpha^2}{Q^4 x}F_2(x,Q^2)\left[1-y-\frac{y^2\gamma^2}{4}+\frac{y^2(1+\gamma^2)}{2(1+R(x,Q^2))}\right].$$

The structure functions $R(x,Q2)$ and $F_2(x,Q^2)$ have been measured by the well-known collaborations SLAC-MIT, EMC, BCDMS, NMC, ZEUS, H_1 and others.

By definition, the structure functions F_1 and F_2 are pure phenomenological. Their physics interpretations can be given only within certain models. In QPM of nucleons IDIS is represented by the diagram in Fig.1.2 (b) in which the virtual photon is absorbed by the nucleon's constituent quark carrying fraction x of the nucleon momentum. In the QCD improved QPM, the quark can emit a gluon before or after absorption. Then

$$F_2(x, Q^2) = x\sum_q e^2_q\,[\mathbf{q}(x, Q^2) + anti\text{-}\mathbf{q}(x, Q^2)],\ q=u, d, s,$$

where e_q is the charge of the quark. From the global QCD analysis of all DIS data one can find PDFs $f^a{}_1$ (the superscript a is usually omitted) in the non-polarized nucleon for each parton (Fig.1.3).

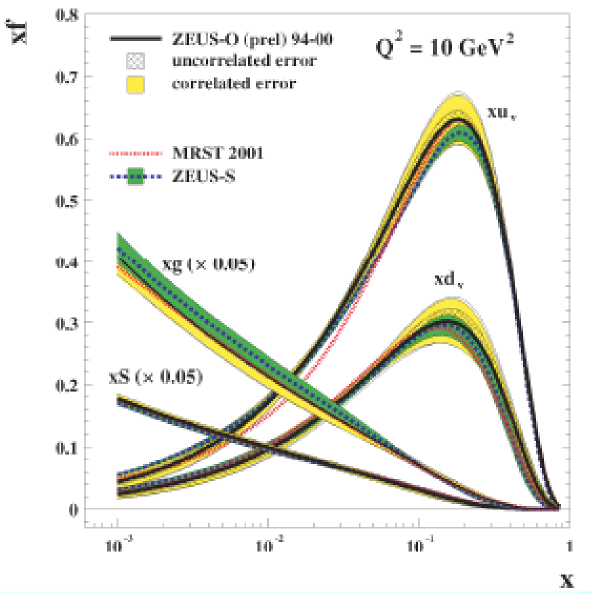

Fig.1.3: *parton (density) distributions in non-polarized nucleons at Q^2=10 GeV^2 vs. x.*

The spin-dependent part of the cross section, σ^{pol}, can be extracted from so-called asymmetries which are proportional to the difference between cross sections for two opposite target polarizations. The difference between cross sections, $\Delta\sigma_{//}$, for two opposite longitudinal target polarizations is given by the expression:

$$\Delta\sigma_{//} \equiv \Delta\left(\frac{d^2\sigma^{pol}_{//}}{dxdQ^2}\right) = \frac{16\pi\alpha^2 y}{Q^4}\left[\left(1-\frac{y}{2}-\frac{y^2\gamma^2}{4}\right)g_1 - \frac{y\gamma^2}{2}g_2\right],$$

The polarized part of the cross section, σ^{pol}, is small compared to σ^{unp} and its contribution to the experimental counting rate is further reduced by incomplete beam and target polarizations. So, to separate σ^{pol}, instead of measurements of differences between the cross sections, experiments measure asymmetries. The longitudinal asymmetry, $A_{//}$, is defined as

$$A_{//} = \frac{\Delta\sigma_{//}}{2\sigma^{unp}} = \frac{\sigma^{\rightarrow\Rightarrow} - \sigma^{\rightarrow\Leftarrow}}{\sigma^{\rightarrow\Leftarrow} + \sigma^{\rightarrow\Rightarrow}} \quad .$$

The arrows $\rightarrow$ and $\Rightarrow$ indicate the directions of the incident lepton and the polarisation of the target, respectively. The asymmetry $A_{//}$ is related to the virtual photon asymmetries A_1 and A_2:

$$A_{//} = D\,(A_1 + \eta A_2) \approx DA_1.$$

Here

$$D = \frac{y(2-y)(1+\gamma^2 y/2)}{(1+\gamma^2)[y^2(1-2m_e^2/Q^2) + 2(1-y-\gamma^2 y^2/4)(1+R)/(1+\gamma^2)]},$$

$$A_2 = \gamma\,(g_1 + g_2)/F_1.$$

The A_2 is estimated to be small. So, using the above mentioned expressions for σ^{pol} *and* σ^{unp}, in the first approximation one can obtain a relation connecting $A_{//}$ and g_1:

$$A_{//}/D \approx A_1 \approx (g_1 - \gamma^2 g_2)/F_1 \approx g_1/F_1, \text{ term } \gamma^2 g_2 \text{ is small.}$$

The F_1 is expressed in terms of structure functions $F_2(x, Q^2)$ and $R(x, Q^2)$:

$$F_1 = \frac{1+\gamma^2}{2x(1+R)} \cdot F_2$$

In QPM, IDIS is represented by the diagram in Fig.1.2 (b, c): the virtual photon is absorbed by the constituent quark carrying the fraction x of the nucleon momentum. Due to conservation of the total angular momentum, this photon can be absorbed only by a quark having the spin oriented in the opposite direction to the photon angular momentum. Taking this into account, one can obtain the QPM expression for virtual photon asymmetry A_1:

$$A_1^p = \frac{\sigma_{1/2}^p - \sigma_{3/2}^p}{\sigma_{1/2}^p + \sigma_{3/2}^p} = \frac{\sum e_i^2 \left[q_i^{\uparrow}(x) - q_i^{\downarrow}(x)\right]}{\sum e_i^2 \left[q_i^{\uparrow}(x) + q_i^{\downarrow}(x)\right]}.$$

In this expression $\sigma_{1/2}$ and $\sigma_{3/2}$ are absorption cross sections of the virtual photon (γ^*) by the nucleon with the total photon-nucleon angular momentum along the γ^* axis equal to 1/2 or 3/2, respectively. The denominator of this expression by definition is equal to the non-polarized structure function $F_1^p(x)$. So, the numerator is associated with the structure function g_1:

$$g_1(x) = \sum_i e_i^2 \left[q_i^{\uparrow}(x) - q_i^{\downarrow}(x)\right].$$

It gives information on the quark spin orientation (helicity) with respect to the nucleon spin in the longitudinally polarized nucleon.

The structure functions $g^p{}_1(x, Q^2)$ and $g^d{}_1(x, Q^2)$ for protons and deuterons have been determined from inclusive asymmetries A_1 measured by various collaborations at SLAC, CERN, DESY, JLAB. The summary of present g_1 data is shown in Fig.1.4 [2]. The data are in very good agreement between themselves and with the QCD NLO predictions.

Inclusive and semi-inclusive asymmetries for proton and deuteron of the type shown in Fig.1.5 permit to determine quark helicity distributions Δq, Fig.1.5, right by using the following expression:

$$A_1^{h\,(p/d)}(x,z,Q^2) \approx \frac{\sum_q e_q^2 \Delta q(x,Q^2) D_q^h(z,Q^2)}{\sum_q e_q^2 q(x,Q^2) D_q^h(z,Q^2)}$$

in which parameterizations of non-polarized quark distributions $q(x, Q^2)$ and quark fragmentation functions (***FF***) $D^h{}_q(z, Q^2)$ measured in other experiments are used. The precision of this determination depends very much on the precision of the FFs. This is especially important for the strange quarks. Data shown in Fig.1.5 give only values for $x\Delta S$, where S is the sum of strange quarks and anti-quarks.

One can estimate the quark contributions to the nucleon spin integrating the helicity distributions over the covered x-range. As it is known, the longitudinal projection of the nucleon spin is equal to ½ in units of the Max Plank constant. In QPM it is defined as a sum of contributions of quarks, gluons and their orbital momenta:

$$S_N = ½ = ½\,(\Delta\Sigma + \Delta G + L^q_z + L^g_z).$$

The present value of the quark contributions determined from the helicity distributions amounts to about 33% of the S_N.This result confirms with high precision the original EMC observation that the quarks contribute little to the total nucleon spin (spin crisis). The COMPASS collaboration in the separate measurements, Fig.1.6, has shown that the gluons contribute to the nucleon spin even smaller than that of quarks, almost zero. This is confirmed by the RHIC experiments. At the present knowledge, the nucleon spin crisis can be solved by future measurements of Generalized Parton Distributions (GPD) accounting also for orbital momenta of nucleon constituents.

Similarly to the non-polarized PDF, the latest QCD analysis [3] of the $g^p_1(x, Q^2)$ and $g^d_1(x, Q^2)$ data produce the helicity distribution PDF g^a_1 (Fig.1.7).

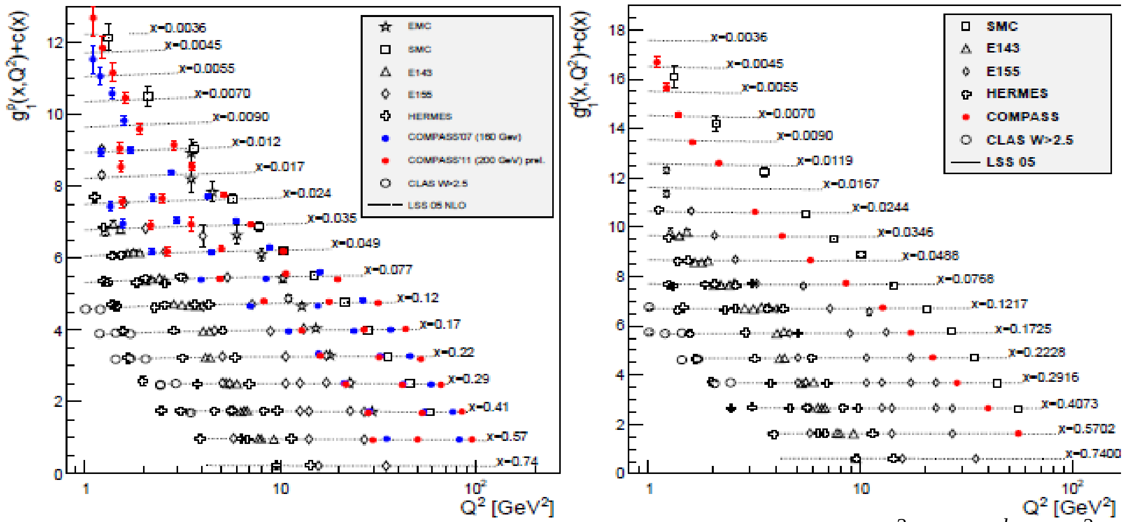

***Fig.1.4:** summary of the world data on the structure functions $g^p_1(x, Q^2)$ and $g^d_1(x, Q^2)$.*

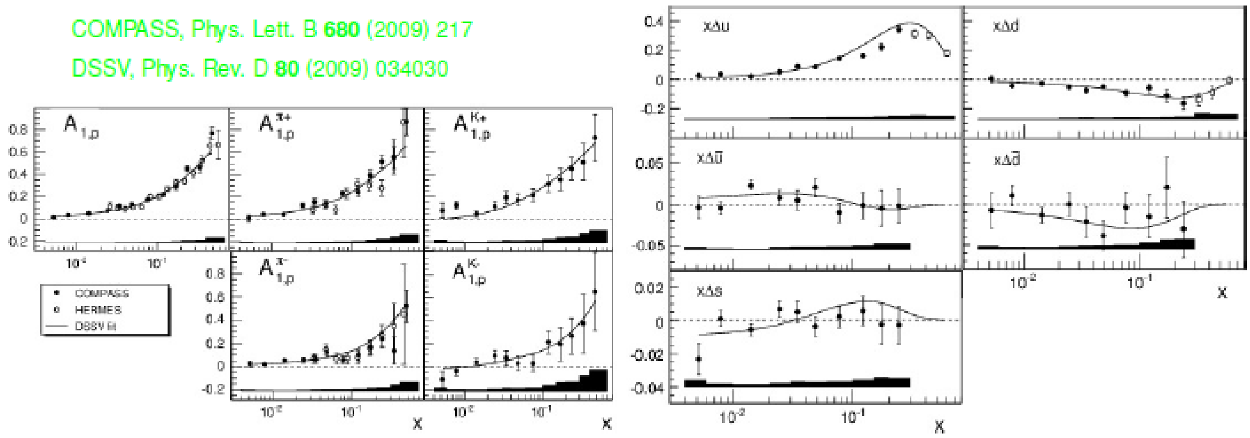

***Fig.1.5: left**: inclusive and semi-inclusive asymmetries for protons. **Right**: quark helicity PDFs.*

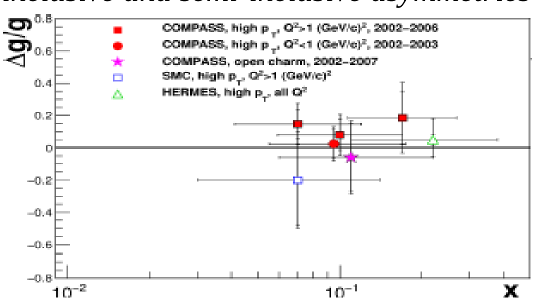

***Fig.1.6:** direct measurements of the gluon polarization in the nucleon.*

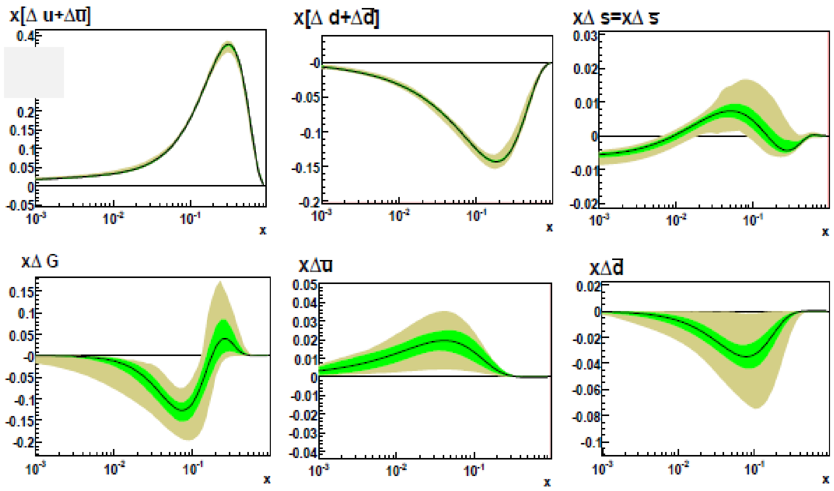

Fig.1.7: *parton helicity distributions in the longitudinally polarized nucleon.*

1.3. TMD PDFs.

The new TMD PDFs are chiral odd and can be measured only in the SIDIS or DY processes, Fig.1.8. So far data have been obtained for the polarized nucleon only from SIDIS by the HERMES and COMPASS collaborations. Polarized TMD PDFs from the DY processes in πp interactions are to be measured at COMPASS-II. There is a real opportunity and challenge to study TMD PDFs at NICA in polarized *pp* and *pd* collisions (see Section2.1).

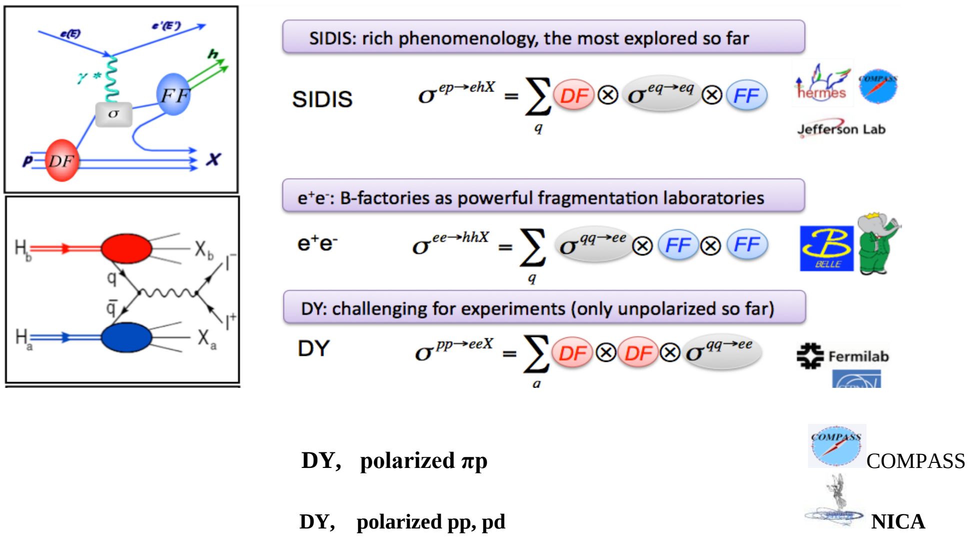

Fig.1.8: reactions for TMD PDF studies.

In SIDIS, the chiral TMD PDFs can be obtained studying the azimuthal modulations of hadrons which are sensitive to convolution of PDF with the corresponding FF:

- Transversity: $A_{UT}^{sin(\phi_h+\phi_S)} \propto h_1 \otimes H_1^\perp$
- Sivers: $A_{UT}^{sin(\phi_h-\phi_S)} \propto f_{1T}^\perp \otimes D_1$
- Pretzelosity: $A_{UT}^{sin(3\phi_h-\phi_S)} \propto h_{1T}^\perp \otimes H_1^\perp$
- Boer-Mulders: $A_{UU}^{cos(2\phi_h)} \propto h_1^\perp \otimes H_1^\perp$
- Worm-Gears: $A_{UL}^{sin(2\phi_h)} \propto h_{1L}^\perp \otimes H_1^\perp$; $A_{LT}^{cos(\phi_h-\phi_S)} \propto g_{1T}^\perp \otimes D_1$.

The first and second subscript labeling azimuthal modulations indicate beam and target polarizations; ϕ_h and ϕ_S are the azimuthal angles of produced hadron and initial nucleon spin, defined with respect to the direction of the virtual photon in the lepton scattering plane; $H^{\perp}_{1}$ is the Collins FF which describes the distribution of non-polarized hadrons in the fragmentation of the transversely polarized quark and D_1 is the non-polarized k_T dependent FF. The Collins FF is chiral-odd; it is a partner of transversity. The status of these PDFs measurement is summarized in [4] and updated in [5].

1.3.1. Transversity PDF h_1.

The azimuthal modulations of hadrons' production measured in the SIDIS process $l+p\ (d) \rightarrow l+h+X$ on polarized protons and deuterons have been observed by the HERMES and COMPASS collaborations. The proton data are shown in Fig.1.9. The COMPASS deuteron data on asymmetries are compatible with zero due to cancelations between the *u* and *d* quarks contributions. The Collins FF has been measured recently by the BELLE collaboration at KEK. The global analysis of the HERMES, COMPASS and BELLE data allowed obtaining the transversity distributions for *u* and *d* quarks (Fig.1.9, right) although still with rather large uncertainties.

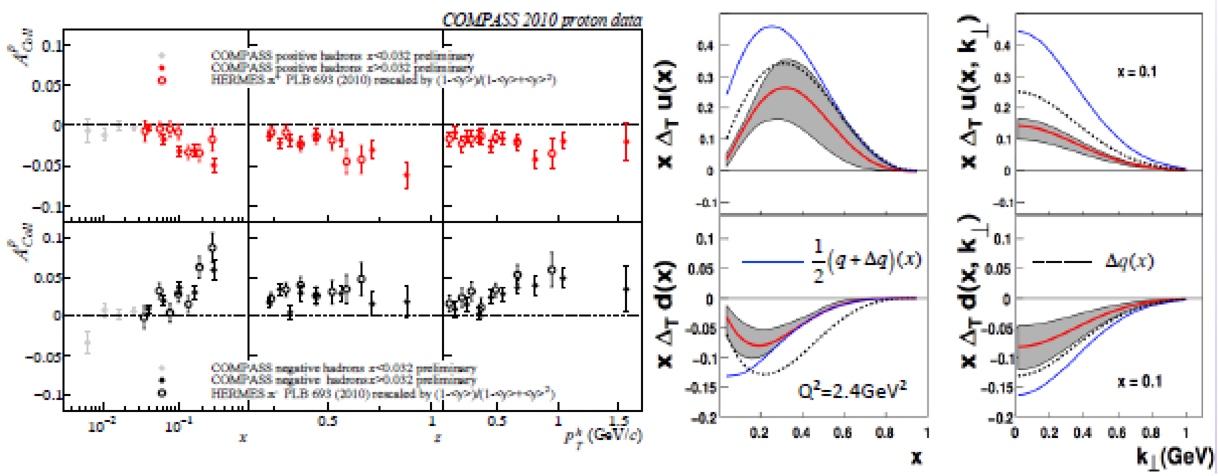

***Fig.1.9: Left**: Collins asymmetry from COMPASS & HERMES. **Right**: transversity PDFs extracted from the global analysis.*

1.3.2. Sivers PDF $f^{\perp}_{1T}$.

The Sivers correlation between the transverse nucleon spin and transverse momentum of its partons was originally proposed to explain large single-spin asymmetries observed in the hadron productions at Protvino and Fermilab. Later on, possibility of the Sivers effect existence has been confirmed for the Wilson-line TMD PDFs to enforce gauge invariance of QCD. The final state interactions in SIDIS (or initial state interactions in DY) allowed for the non-zero T-odd Sivers PDFs but they must have opposite signs in SIDIS and DY.

Sivers asymmetries have been measured by the HERMES, COMPASS and JLAB collaborations on proton, deuteron, and ^{3}He targets, respectively. Definite signals are observed for protons (Fig.1.10). Because of cancelations between *u* and *d* quark contributions, Sivers asymmetries for the isoscalar targets are compatible with zero. From the global analysis of the HERMES and COMPASS data, the Sivers TMD PDFs for *u* and *d* quarks are determined (Fig.1.10, right).

1.3.3. Boer-Mulders $h^{\perp}_{1}$, worm-gear-T ($g^{\perp}_{1T}$) and worm-gear-L ($h^{\perp}_{1L}$) PDFs.

The ***Boer-Mulders*** TMD PDF, like the Sivers one, is T-odd and must have opposite signs once measured in SIDIS or DY. It can be observed (in convolution with the Collins FF) from the *Cos (2ϕ)* azimuthal modulation of hadrons produced in the non-polarized SIDIS. Signals of this modulation have been seen by HERMES and COMPASS.

The ***worm-gear-T*** PDF characterizing correlation between longitudinally polarized quarks inside a transversely polarized nucleon is very interesting. It is chiral-even and can be observed in SIDIS convoluted with non-polarized FF studying $Cos\ (\phi_h - \phi_S)$ modulation in hadron production by longitudinally polarized leptons on the transversely polarized target. Preliminary results were obtained by COMPASS and HERMES (Fig.1.11).

Attempts to see the ***worm-gear-L*** PDF were made by COMPASS. No signal is observed within the available statistical accuracy.

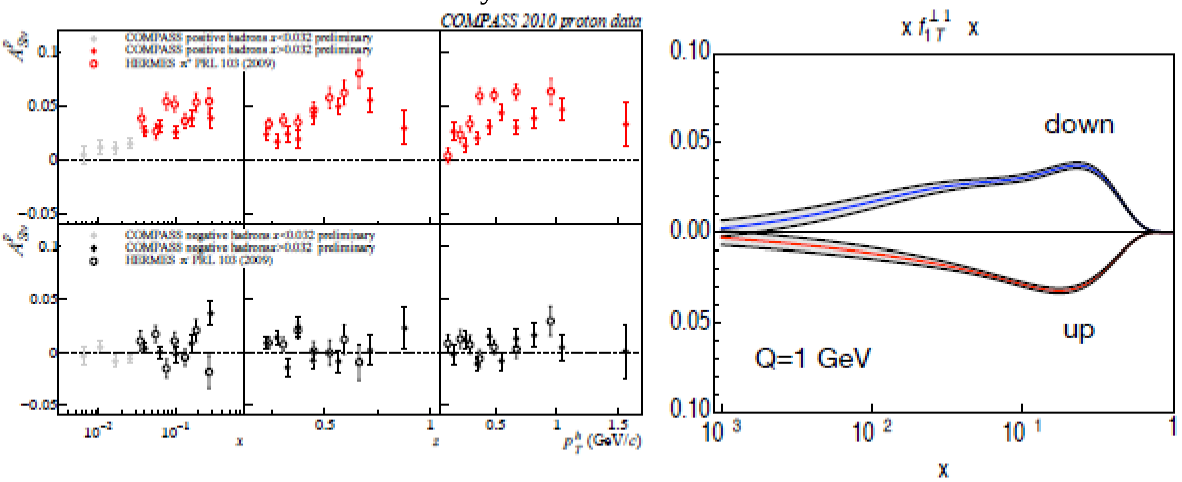

Fig.1.10: left*: Sivers asymmetry from COMPASS and HERMES.* ***Right****: Sivers PDFs for the u and d quarks determined from the global analysis.*

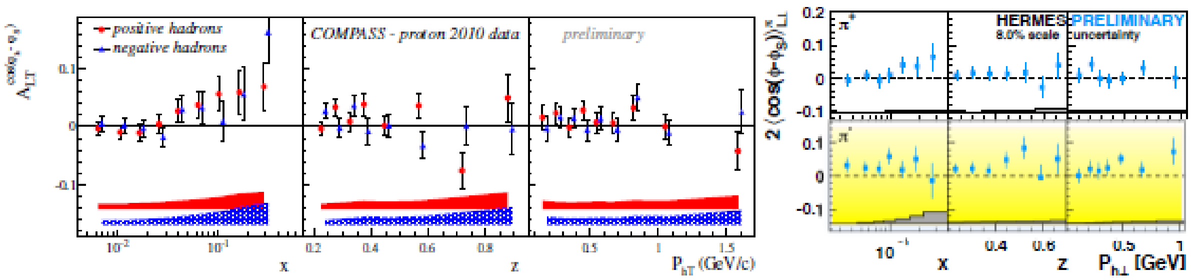

Fig.1.11: *preliminary data on modulations characterizing the worm-gear-T TMD PDF.* ***Left****: COMPASS,* ***right****: HERMES.*

1.3.4. Pretzelosity PDF $h^{\perp}_{1T}$.

Pretzelosity has been looked for by COMPASS. The $sin\ (3\phi_h - \phi_S)$ asymmetry modulations in hadrons' production are found to be compatible with zero within the available statistical accuracy. So, no signal of pretzelosity is observed yet.

Concluding the Section 1.3, one can summarize that the collinear and TMD PDFs are necessary for complete description of the nucleon structure at the level of twist-2 approximation. Its precision measurement at NICA can be the main subject of the NICA SPD spin program.

1.4. Other actual problems of high energy physics.

There are actual problems in high energy physics which are partially solved or not solved at all. Among them one can mention the high-p_T behavior of elastic cross sections (Fig.1.12), the high-p_T behavior of the asymmetry A_n in elastic *pp* scattering and inclusive hyperons polarization (Fig.1.13), the deuteron wave function behavior as a function of *k*, (Fig.1.14), and some others.

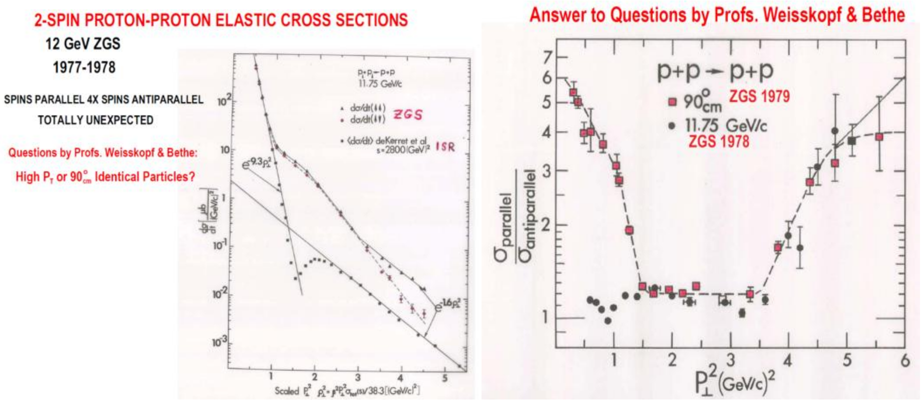

Fig.1.12: *the famous pp elastic scattering data at large* p_T **.**

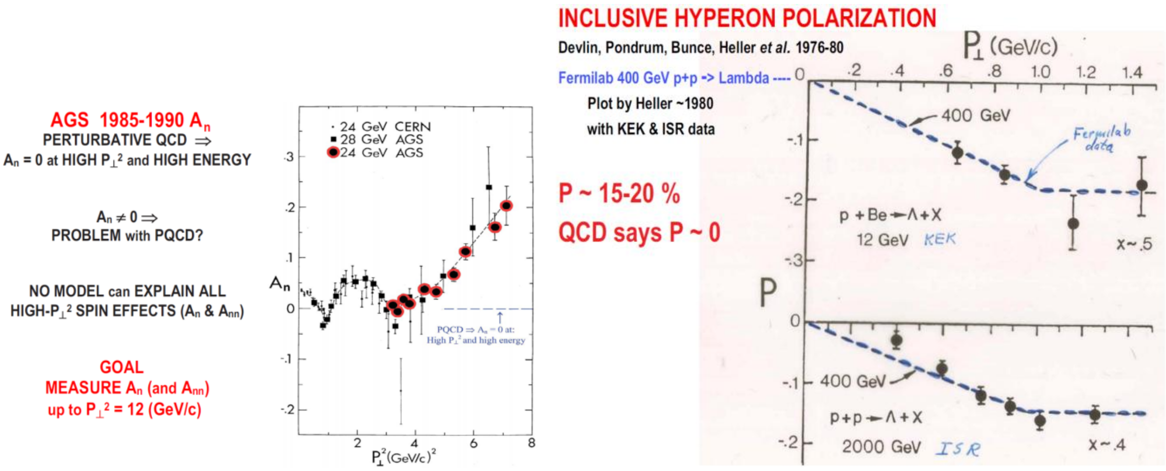

Fig.1.13: right- *the Λ hyperons polarization in inclusive pp reactions.*

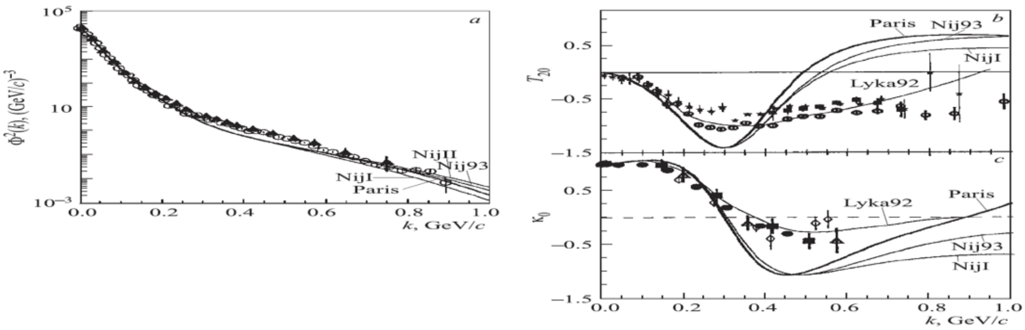

Fig.1.14: *world data on the deuteron wave function.*

2. Physics motivations. (UPDATING)

2.1. Nucleon structure studies using the Drell-Yan mechanism.

2.1.1. The PDFs studies via asymmetry of cross sections.

The Drell-Yan (*DY*) process of the di-lepton production in high-energy hadron-hadron collisions (Fig. 2.1) is playing an important role in the hadron structure studies:

$$H_a(P_a, S_a) + H_b(P_b, S_b) \to l^-(l, \lambda) + l^+(l', \lambda') + X \,, \qquad (2.1.1)$$

where $\boldsymbol{P_a}$ ($\boldsymbol{P_b}$) and $\boldsymbol{S_a}$ ($\boldsymbol{S_b}$) are the momentum and spin of the hadron H_a (H_b), respectively, while $\boldsymbol{l}$ ($\boldsymbol{l'}$) and $\boldsymbol{\lambda}$ ($\boldsymbol{\lambda'}$) are the momentum and spin of the lepton, respectively.

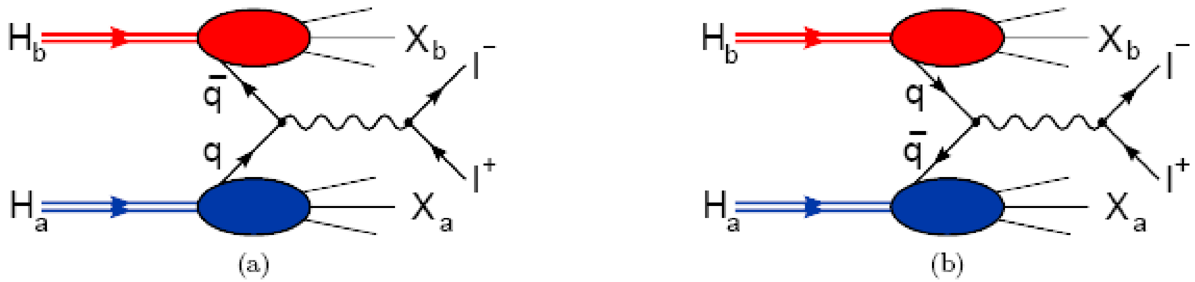

Fig. 2.1: the *parton model diagrams of the di-lepton production in collisions of hadrons* H_a *(*P_a*,*S_a*) with hadrons* H_b *(*P_b*,*S_b*). The constituent quark (anti-quark) of the hadron* H_a *annihilates with constituent anti-quark (quark) of the hadron* H_b *producing the virtual photon which decays into a pair of leptons* $l^{\pm}$ *(electron-positron or* $\mu^{\pm}$*). The hadron spectator systems* X_a *and* X_b *are usually not detected. Both diagrams have to be taken into account.*

The kinematics of the Drell-Yan process can be most conveniently considered in the Collins-Soper (CS) reference frame [1-4], Fig. 2.2. The transition from the hadrons-center-of-mass frame (*cm*-frame) to the CS-frame is described in [1]. The CS-frame includes three intersecting planes. The first one is the *Lepton plane* containing vectors of the lepton momenta, ***l, l'*** (in the lepton rest frame), and the unit vector in the z-direction, $\hat{e}_{z,CS}$,

$$\hat{e}_{z,CS} = (\vec{P}_{a,CS}/|\vec{P}_{a,CS}| - \vec{P}_{b,CS}/|\vec{P}_{a,CS}|)/2\cos\alpha, \quad (\hat{e}_{x,CS} = -(\vec{P}_{a,CS}/|\vec{P}_{a,CS}| + \vec{P}_{b,CS}/|\vec{P}_{a,CS}|)/2\sin\alpha),$$

where tg$\alpha = \boldsymbol{q_T}/q$, $\boldsymbol{q_T}$ *(*$q = l + l'$*,* $q \equiv Q$*)* is the transverse momentum (momentum) of the virtual photon in the *cm*-frame. The second plane, the *Hadron or Collins-Soper* plane, contains the momentum of colliding hadrons, P_a, P_b , and vector $\hat{h}$ – is the unit vector in the direction of the photon transverse momentum, $\hat{h} = \vec{q}_T/q_T$, and the third plane – *Polarization plane* – contains the polarization vector $S \equiv \boldsymbol{S_T}$ ($\boldsymbol{S_{aT}}$, $\boldsymbol{S_{bT}}$) and the unit vector $\hat{e}_{z,CS}$. The ϕ is the azimuthal angle between the *Lepton* and *Hadron* planes; ϕ_S (i.e. ϕ_{Sa} or ϕ_{Sb}) is the angle between the *Lepton* and *Polarization* planes and $\boldsymbol{\theta}$ is the polar angle of $\boldsymbol{l}$ in the CS-frame.

The most complete theoretical analysis of this process, for cases when both hadrons H_a and H_b, in our case protons or deuterons, are polarized or non-polarized, was performed in [5] which we will follow below. Let us consider the regime where $q_T \ll q$. In this region the TMD PDFs enter the description of the DY process in a natural way. Our treatment is restricted to the leading twist, i.e. to the leading order of TMDs expansion in powers of *1/q*. Because of the potential problems of the sub-leading-twist -TMD PDFs- factorization pointed out in Refs. [6, 7], we refrain from including in considerations the twist-3 case. Moreover, we neither take into account higher order hard scattering corrections nor effects associated with soft gluon radiation.

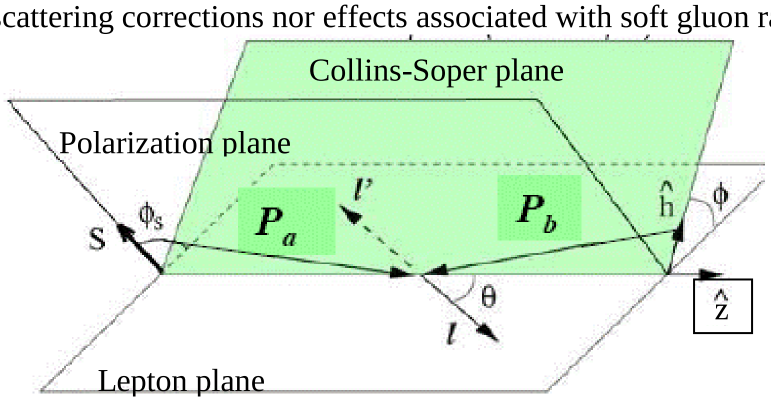

Fig. 2.2: *kinematics of the Drell-Yan process in the Collins-Soper reference frame.*

In this approximation the Eq. (57) of Ref. [5] for the differential cross section of the DY pair's production in the quark-parton model via PDFs is rewritten by us in the more convenient variables with a change of notations of the azimuthal angle polarizations corresponding to Fig.2.2:

$$
\begin{aligned}
&\frac{d\sigma}{dx_a dx_b d^2q_T d\Omega}=\frac{\alpha^2}{4Q^2}\times \\
&\Big\{\Big((1+\cos^2\theta)F_{UU}^{1}+\sin^2\theta\cos 2\phi F_{UU}^{\cos 2\phi}\Big)+S_{aL}\sin^2\theta\sin 2\phi F_{LU}^{\sin 2\phi}+S_{bL}\sin^2\theta\sin 2\phi F_{UL}^{\sin 2\phi} \\
&+\left|\vec{S}_{aT}\right|\Big[\sin(\phi-\phi_{S_a})\big(1+\cos^2\theta\big)F_{TU}^{\sin(\phi-\phi_{S_a})}+\sin^2\theta\Big(\sin(3\phi-\phi_{S_a})F_{TU}^{\sin(3\phi-\phi_{S_a})}+\sin(\phi+\phi_{S_a})F_{TU}^{\sin(\phi+\phi_{S_a})}\Big)\Big] \\
&+\left|\vec{S}_{bT}\right|\Big[\sin(\phi-\phi_{S_b})\big(1+\cos^2\theta\big)F_{UT}^{\sin(\phi-\phi_{S_b})}+\sin^2\theta\Big(\sin(3\phi-\phi_{S_b})F_{UT}^{\sin(3\phi-\phi_{S_b})}+\sin(\phi+\phi_{S_b})F_{UT}^{\sin(\phi+\phi_{S_b})}\Big)\Big] \\
&+S_{aL}S_{bL}\Big[\big(1+\cos^2\theta\big)F_{LL}^{1}+\sin^2\theta\cos 2\phi F_{LL}^{\cos 2\phi}\Big] \qquad (2.1.2) \\
&+S_{aL}\left|\vec{S}_{bT}\right|\Big[\cos(\phi-\phi_{S_b})\big(1+\cos^2\theta\big)F_{LT}^{\cos(\phi-\phi_{S_b})}+\sin^2\theta\Big(\cos(3\phi-\phi_{S_b})F_{LT}^{\cos(3\phi-\phi_{S_b})}+\cos(\phi+\phi_{S_b})F_{LT}^{\cos(\phi+\phi_{S_b})}\Big)\Big] \\
&+\left|\vec{S}_{aT}\right|S_{bL}\Big[\cos(\phi-\phi_{S_a})\big(1+\cos^2\theta\big)F_{TL}^{\cos(\phi-\phi_{S_a})}+\sin^2\theta\Big(\cos(3\phi-\phi_{S_a})F_{TL}^{\cos(3\phi-\phi_{S_a})}+\cos(\phi+\phi_{S_a})F_{TL}^{\cos(\phi+\phi_{S_a})}\Big)\Big] \\
&+\left|\vec{S}_{aT}\right|\left|\vec{S}_{bT}\right|\Big[\big(1+\cos^2\theta\big)\Big(\cos(2\phi-\phi_{S_a}-\phi_{S_b})F_{TT}^{\cos(2\phi-\phi_{S_a}-\phi_{S_b})}+\cos(\phi_{S_b}-\phi_{S_a})F_{TT}^{\cos(\phi_{S_b}-\phi_{S_a})}\Big)\Big] \\
&+\left|\vec{S}_{aT}\right|\left|\vec{S}_{bT}\right|\Big[\sin^2\theta\Big(\cos(\phi_{S_a}+\phi_{S_b})F_{TT}^{\cos(\phi_{S_a}+\phi_{S_b})}+\cos(4\phi-\phi_{S_a}-\phi_{S_b})F_{TT}^{\cos(4\phi-\phi_{Sa}-\phi_{S_b})}\Big)\Big] \\
&+\left|\vec{S}_{aT}\right|\left|\vec{S}_{bT}\right|\Big[\sin^2\theta\Big(\cos(2\phi-\phi_{S_a}+\phi_{S_b})F_{TT}^{\cos(2\phi-\phi_{S_a}+\phi_{S_b})}+\cos(2\phi+\phi_{S_a}-\phi_{S_b})F_{TT}^{\cos(2\phi+\phi_{S_a}-\phi_{S_b})}\Big)\Big]\Big\}
\end{aligned}
$$

where F_j^i are the Structure Functions (SFs) connected to the corresponding PDFs. The SFs depend on four variables $P_a \cdot q$, $P_b \cdot q$, $\boldsymbol{q_T}$ and q^2 or on $\boldsymbol{q_T}$, q^2 and the Bjorken variables of colliding hadrons, x_a , x_b ,

$$x_a=\frac{q^2}{2P_a\cdot q}=\sqrt{\frac{q^2}{s}}e^{y},\ x_b=\frac{q^2}{2P_b\cdot q}=\sqrt{\frac{q^2}{s}}e^{-y},\ \text{ y is the } cm \text{ rapidity.} \qquad (2.1.3)$$

The SFs F_j^i introduced here give more detailed information on the nucleon structure than usual structure functions depending on two variables x_{Bj} and Q^2. Equation (2.1.2) includes 24 leading twist SFs. Each of them is expressed through a weighted convolution, C , of corresponding leading twist TMD PDF in the transverse momentum space,

$$
\begin{aligned}
C\Big[w(\vec{k}_{aT},\vec{k}_{bT})f_1\bar{f}_2\Big]\equiv\frac{1}{N_c}\sum_q e_q^2\int d^2\vec{k}_{aT}d^2\vec{k}_{bT}\delta^2(\vec{q}_T-\vec{k}_{aT}-\vec{k}_{bT})w(\vec{k}_{aT},\vec{k}_{bT})\times \\
\Big[f_{1q}(x_a,\vec{k}_{aT}^2)\bar{f}_{2q}(x_b,\vec{k}_{bT}^2)+\bar{f}_{1q}(x_a,\vec{k}_{aT}^2)f_{2q}(x_b,\vec{k}_{bT}^2)\Big], \qquad (2.1.4)
\end{aligned}
$$

where k_{aT} (k_{bT}) is the transverse momentum of quark in the hadron H_a (H_b) and f_1 (f_2) is a TMD PDF of the corresponding hadron. The particular SF can include a linear combination of several PDFs. Eventually; one can find expressions for all leading twist SFs of **quarks** and **antiquarks** entering Eq. (2.1.2). For the non-polarized hadrons they are:

$$F_{UU}^{1}=C\Big[f_1\bar{f}_1\Big],\quad F_{UU}^{\cos 2\phi}=C\left[\frac{2(\vec{h}\cdot\vec{k}_{aT})(\vec{h}\cdot\vec{k}_{bT})-\vec{k}_{aT}\cdot\vec{k}_{bT}}{M_aM_b}h_1^{\perp}\bar{h}_1^{\perp}\right], \qquad (2.1.5)$$

for the single polarized hadrons (protons or deuterons):

$$F_{LU}^{\sin 2\phi}=C\left[\frac{2(\vec h\cdot\vec k_{aT})(\vec h\cdot\vec k_{bT})-\vec k_{aT}\cdot\vec k_{bT}}{M_aM_b}h_{1L}^{\perp}\bar h_1^{\perp}\right],\quad F_{UL}^{\sin 2\phi}=-C\left[\frac{2(\vec h\cdot\vec k_{aT})(\vec h\cdot\vec k_{bT})-\vec k_{aT}\cdot\vec k_{bT}}{M_aM_b}h_1^{\perp}\bar h_{1L}^{\perp}\right],$$

$$F_{UT}^{\sin(\phi-\phi_{S_b})}=C\left[\frac{\vec h\cdot\vec k_{bT}}{M_b}f_1\bar f_{1T}^{\perp}\right],\qquad F_{TU}^{\sin(\phi-\phi_{S_a})}=-C\left[\frac{\vec h\cdot\vec k_{aT}}{M_a}f_{1T}^{\perp}\bar f_1\right],$$

$$F_{TU}^{\sin(3\phi-\phi_{S_a})}=C\left[\frac{2(\vec h\cdot\vec k_{aT})[2(\vec h\cdot\vec k_{aT})(\vec h\cdot\vec k_{bT})-\vec k_{aT}\cdot\vec k_{bT}]-\vec k_{aT}^2(\vec h\cdot\vec k_{bT})}{2M_a^2M_b}h_{1T}^{\perp}\bar h_1^{\perp}\right],$$

$$F_{UT}^{\sin(3\phi-\phi_{S_b})}=-C\left[\frac{2(\vec h\cdot\vec k_{bT})[2(\vec h\cdot\vec k_{aT})(\vec h\cdot\vec k_{bT})-\vec k_{aT}\cdot\vec k_{bT}]-\vec k_{bT}^2(\vec h\cdot\vec k_{aT})}{2M_aM_b^2}h_1^{\perp}\bar h_{1T}^{\perp}\right],$$

$$F_{TU}^{\sin(\phi+\phi_{S_a})}=C\left[\frac{\vec h\cdot\vec k_{bT}}{M_b}h_1\bar h_1^{\perp}\right],\quad F_{UT}^{\sin(\phi+\phi_{S_b})}=-C\left[\frac{\vec h\cdot\vec k_{aT}}{M_a}h_1^{\perp}\bar h_1\right],$$

(2.1.6)

for the both polarized hadrons:

$$F_{LL}^{1}=-C\left[g_{1L}\bar g_{1L}\right],\quad F_{LL}^{\cos 2\phi}=C\left[\frac{2(\vec h\cdot\vec k_{aT})(\vec h\cdot\vec k_{bT})-\vec k_{aT}\cdot\vec k_{bT}}{M_aM_b}h_{1L}^{\perp}\bar h_{1L}^{\perp}\right],$$

$$F_{LT}^{\cos(\phi-\phi_{S_b})}=-C\left[\frac{\vec h\cdot\vec k_{bT}}{M_b}g_{1L}\bar g_{1T}\right],\qquad F_{TL}^{\cos(\phi-\phi_{S_a})}=-C\left[\frac{\vec h\cdot\vec k_{aT}}{M_a}g_{1T}\bar g_{1L}\right],$$

$$F_{TL}^{\cos(\phi+\phi_{S_a})}=C\left[\frac{\vec h\cdot\vec k_{bT}}{M_b}h_1\bar h_{1L}^{\perp}\right],\quad F_{LT}^{\cos(\phi+\phi_{S_b})}=C\left[\frac{\vec h\cdot\vec k_{aT}}{M_a}h_{1L}^{\perp}\bar h_1\right],$$

$$F_{LT}^{\cos(3\phi-\phi_{S_b})}=C\left[\frac{2(\vec h\cdot\vec k_{bT})[2(\vec h\cdot\vec k_{aT})(\vec h\cdot\vec k_{bT})-\vec k_{aT}\cdot\vec k_{bT}]-\vec k_{bT}^2(\vec h\cdot\vec k_{aT})}{2M_aM_b^2}h_{1L}^{\perp}\bar h_{1T}^{\perp}\right],$$

$$F_{TL}^{\cos(3\phi-\phi_{S_a})}=C\left[\frac{2(\vec h\cdot\vec k_{aT})[2(\vec h\cdot\vec k_{aT})(\vec h\cdot\vec k_{bT})-\vec k_{aT}\cdot\vec k_{bT}]-\vec k_{aT}^2(\vec h\cdot\vec k_{bT})}{2M_a^2M_b}h_{1T}^{\perp}\bar h_{1L}^{\perp}\right],$$

$$F_{TT}^{\cos(2\phi-\phi_{S_a}-\phi_{S_b})}=C\left[\frac{2(\vec h\cdot\vec k_{aT})(\vec h\cdot\vec k_{bT})-\vec k_{aT}\cdot\vec k_{bT}}{2M_aM_b}(f_{1T}^{\perp}\bar f_{1T}^{\perp}-g_{1T}\bar g_{1T})\right],\tag{2.1.7}$$

$$F_{TT}^{\cos(\phi_{S_b}-\phi_{S_a})}=-C\left[\frac{\vec k_{aT}\cdot\vec k_{bT}}{2M_aM_b}(f_{1T}^{\perp}\bar f_{1T}^{\perp}+g_{1T}\bar g_{1T})\right],\qquad F_{TT}^{\cos(\phi_{S_b}+\phi_{S_a})}=C\left[h_1\bar h_1\right],$$

$$F_{TT}^{\cos(2\phi-\phi_{S_a}+\phi_{S_b})}=C\left[\frac{2(\vec h\cdot\vec k_{aT})^2-\vec k_{aT}^2}{2M_a^2}h_{1T}^{\perp}\bar h_1\right],\quad F_{TT}^{\cos(2\phi+\phi_{S_a}-\phi_{S_b})}=C\left[\frac{2(\vec h\cdot\vec k_{bT})^2-\vec k_{bT}^2}{2M_b^2}h_1\bar h_{1T}^{\perp}\right],$$

$$F_{TT}^{\cos(4\phi-\phi_{Sa}-\phi_{Sb})}=C\left[\left(\frac{4(\vec h\cdot\vec k_{aT})(\vec h\cdot\vec k_{bT})[2(\vec h\cdot\vec k_{aT})(\vec h\cdot\vec k_{bT})-\vec k_{aT}\cdot\vec k_{bT}]}{4M_a^2M_b^2}\right.\right.$$
$$\left.\left.+\frac{\vec k_{aT}^2\vec k_{bT}^2-2\vec k_{aT}^2(\vec h\cdot\vec k_{bT})^2-2\vec k_{bT}^2(\vec h\cdot\vec k_{aT})^2}{4M_a^2M_b^2}\right)h_{1T}^{\perp}\bar h_{1T}^{\perp}\right].$$

Note that the exchange $H_a \leftrightarrow H_b$ in these expressions leads to the reversal of the z-direction which, in particular, implies exchanges:

$$\phi_{S_a} \leftrightarrow -\phi_{Sb},\ \phi \to -\phi,\ \theta \to \pi - \theta. \qquad (2.1.8)$$

The cross section (2.1.2) cannot be measured directly because there is no single beam containing particles with the U, L and T polarization. To measure SFs entering this equation one can use the following procedure: first, integrate Eq. (2.1.2) over the azimuthal angle ϕ, second, following the SIDIS practice, to measure azimuthal asymmetries of the DY pair's production cross sections.

The integration over the azimuthal angle ϕ gives:

$$\sigma_{\rm int} \equiv \frac{d\sigma}{dx_a dx_b d^2 q_T d\cos\theta} = \frac{\pi\alpha^2}{2q^2} \times \left(1+\cos^2\theta\right)\Big[F_{UU}^1 + S_{aL}S_{bL}F_{LL}^1$$
$$+\left|\vec{S}_{aT}\right|\left|\vec{S}_{bT}\right|\left(\cos(\phi_{S_b}-\phi_{S_a})F_{TT}^{\cos(\phi_{S_b}-\phi_{S_a})} + D\cos(\phi_{S_a}+\phi_{S_b})F_{TT}^{\cos(\phi_{S_a}+\phi_{S_b})}\right)\Big] \qquad (2.1.9)$$

The azimuthal asymmetries can be calculated as ratios of cross sections differences to the sum of the integrated over ϕ cross sections. The numerator of the ratio is calculated as a difference of the DY pair's production cross sections in the collision of hadrons H_a and H_b with different polarizations. The difference is considered as a function of the azimuthal angle ϕ *and* q_T, first in the whole region of $\boldsymbol{x_a}$ and $\boldsymbol{x_b}$, and then in bins of $\boldsymbol{x_a}$, $\boldsymbol{x_b}$. The denominator of the ratio is calculated as a sum of $\sigma_{\rm int}$'s calculated for the same hadron polarizations and same $\boldsymbol{x_a}$, $\boldsymbol{x_b}$ regions as in numerator.

The azimuthal distribution of DY pair's production in non-polarized collisions, A_{UU}, and azimuthal asymmetries of the cross sections in polarized collisions given by expressions (2.1.10) can be measured. In these expressions $D = \sin^2\theta / (1+\cos^2\theta)$ is the depolarization factor and $A^i_{jk} = F^i_{jk}/F^1_{UU}$ with the SFs defined in Eqs. (2.1.5-7). The superscripts of the σ^{pq} mean:
$\to(\leftarrow)$ – for positive (negative) longitudinal beam polarization in the direction of $\boldsymbol{P}_{\boldsymbol{a}\,cm}$;
$\uparrow(\downarrow)$ – for transverse beam polarization with the azimuthal angle ϕ_{Sa} or ϕ_{Sb} ($\phi_{Sa}+\pi$ or $\phi_{Sb}+\pi$);
0 – for the non-polarized hadron H_a or H_b. Applying the Fourier analysis to the measured asymmetries, one can separate each of all ratios $A^i_{jk} = F^i_{jk}/F^1_{UU}$ entering Eq. (2.1.10). This will be the ultimate task of the proposed experiments. Extraction of different TMD PDFs from these ratios is a task of the global theoretical analysis (a challenge for the theoretical community) since each of the SFs F^i_{jk} is a result of convolutions of different TMD PDFs in the quark transverse momentum space. For this purpose one needs either to assume a factorization of the transverse momentum dependence for each TMD PDFs, having definite (usually Gaussian) form with some fitting parameters [8], or to transfer F^i_{jk} to impact parameter representation and to use the Bessel weighted TMD PDFs [9].

A number of conclusions can be drawn comparing some asymmetries to be measured. Let us compare the measured asymmetries A_{LU} and A_{UL} and assume that during these measurements the beam polarizations are equal, i.e. $|S_{aL}|=|S_{bL}|$ and hadrons a,b are identical. Then one can intuitively expect that the integrated over x_a and x_b asymmetries $A_{LU} = A_{UL}$. Similarly, comparing the asymmetries A_{TU} and A_{UT} or A_{TL} and A_{LT} one can expect that $A^1{}_{TU} = A^1{}_{UT}$ and $A^1{}_{TL} = A^1{}_{LT}$. Tests of these expectations would be a good check of the parton model approximations.

We close this section with following comments.

1. The Structure Functions F^i_j depend on the variables (x_a, x_b, q_T, q^2). Instead of q_T one may also work with the transverse momentum of one of the hadrons in the CS-frame.

2. Eqs. (2.1.5 - 2.1.7) define 24 SFs out of the 48 [5]. This means that in the considered kinematic region $q_T \ll q$ there is exactly half of the total leading twist SFs.

3. The Structure Functions in Eq. (2.1.2) are understood in the CS-frame. Exactly the same expressions for SFs can be obtained in the Gottfried-Jackson frame, because difference between them is of the order of $O\,(q_T/q)$.

$$
\begin{aligned}
A_{UU} &\equiv \frac{\sigma^{00}}{\sigma^{00}_{\rm int}} = \frac{1}{2\pi}\left(1 + D\cos 2\phi A_{UU}^{\cos 2\phi}\right) \\
A_{LU} &\equiv \frac{\sigma^{\to 0} - \sigma^{\leftarrow 0}}{\sigma^{\to 0}_{\rm int} + \sigma^{\leftarrow 0}_{\rm int}} = \frac{|S_{aL}|}{2\pi} D \sin 2\phi A_{LU}^{\sin 2\phi} \\
A_{UL} &\equiv \frac{\sigma^{0\to} - \sigma^{0\leftarrow}}{\sigma^{0\to}_{\rm int} + \sigma^{0\leftarrow}_{\rm int}} = \frac{|S_{bL}|}{2\pi} D \sin 2\phi A_{UL}^{\sin 2\phi} \\
A_{TU} &\equiv \frac{\sigma^{\uparrow 0} - \sigma^{\downarrow 0}}{\sigma^{\uparrow 0}_{\rm int} + \sigma^{\downarrow 0}_{\rm int}} = \frac{|\vec S_{aT}|}{2\pi}\left[A_{TU}^{\sin(\phi-\phi_{S_a})} \sin(\phi-\phi_{S_a}) + D\left(A_{TU}^{\sin(3\phi-\phi_{S_a})} \sin(3\phi-\phi_{S_a}) + A_{TU}^{\sin(\phi+\phi_{S_a})} \sin(\phi+\phi_{S_a})\right)\right] \\
A_{UT} &\equiv \frac{\sigma^{0\uparrow} - \sigma^{0\downarrow}}{\sigma^{0\uparrow}_{\rm int} + \sigma^{0\downarrow}_{\rm int}} = \frac{|\vec S_{bT}|}{2\pi}\left[A_{UT}^{\sin(\phi-\phi_{S_b})} \sin(\phi-\phi_{S_b}) + D\left(A_{UT}^{\sin(3\phi-\phi_{S_b})} \sin(3\phi-\phi_{S_b}) + A_{UT}^{\sin(\phi+\phi_{S_b})} \sin(\phi+\phi_{S_b})\right)\right] \\
A_{LL} &\equiv \frac{\sigma^{\to\to} + \sigma^{\leftarrow\leftarrow} - \sigma^{\to\leftarrow} - \sigma^{\leftarrow\to}}{\sigma^{\to\to}_{\rm int} + \sigma^{\leftarrow\leftarrow}_{\rm int} + \sigma^{\to\leftarrow}_{\rm int} + \sigma^{\leftarrow\to}_{\rm int}} = \frac{|S_{aL} S_{bL}|}{2\pi}\left(A_{LL}^{1} + D A_{LL}^{\cos 2\phi} \cos 2\phi \right) \\
A_{TL} &\equiv \frac{\sigma^{\uparrow\to} + \sigma^{\downarrow\leftarrow} - \sigma^{\downarrow\to} - \sigma^{\uparrow\leftarrow}}{\sigma^{\uparrow\to}_{\rm int} + \sigma^{\downarrow\leftarrow}_{\rm int} + \sigma^{\downarrow\to}_{\rm int} + \sigma^{\uparrow\leftarrow}_{\rm int}} = \frac{|\vec S_{aT}|\, S_{bL}}{2\pi}\left[A_{TL}^{\cos(\phi-\phi_{S_a})} \cos(\phi-\phi_{S_a}) + D \begin{pmatrix} A_{TL}^{\cos(3\phi-\phi_{S_a})} \cos(3\phi-\phi_{S_a}) \\ + A_{TL}^{\cos(\phi+\phi_{S_a})} \cos(\phi+\phi_{S_a}) \end{pmatrix} \right]
\end{aligned}
$$

$$
\begin{aligned}
A_{LT} &\equiv \frac{\sigma^{\to\uparrow} + \sigma^{\leftarrow\downarrow} - \sigma^{\to\downarrow} - \sigma^{\leftarrow\uparrow}}{\sigma^{\to\uparrow}_{\rm int} + \sigma^{\leftarrow\downarrow}_{\rm int} + \sigma^{\to\downarrow}_{\rm int} + \sigma^{\leftarrow\uparrow}_{\rm int}} = \frac{S_{aL}\, |\vec S_{bT}|}{2\pi}\left[A_{LT}^{\cos(\phi-\phi_{S_b})} \cos(\phi-\phi_{S_b}) + D \begin{pmatrix} A_{LT}^{\cos(3\phi-\phi_{S_b})} \cos(3\phi-\phi_{S_b}) \\ + A_{LT}^{\cos(\phi+\phi_{S_b})} \cos(\phi+\phi_{S_b}) \end{pmatrix} \right] \\
A_{TT} &\equiv \frac{\sigma^{\uparrow\uparrow} + \sigma^{\downarrow\downarrow} - \sigma^{\uparrow\downarrow} - \sigma^{\downarrow\uparrow}}{\sigma^{\uparrow\uparrow}_{\rm int} + \sigma^{\downarrow\downarrow}_{\rm int} + \sigma^{\uparrow\downarrow}_{\rm int} + \sigma^{\downarrow\uparrow}_{\rm int}} = \frac{|\vec S_{aT}|\,|\vec S_{bT}|}{2\pi}\Big[A_{TT}^{\cos(2\phi-\phi_{S_a}-\phi_{S_b})} \cos(2\phi-\phi_{S_a}-\phi_{S_b}) + A_{TT}^{\cos(\phi_{S_b}-\phi_{S_a})} \cos(\phi_{S_b}-\phi_{S_a}) \\
&+ D\Big(A_{TT}^{\cos(\phi_{S_b}+\phi_{S_a})} \cos(\phi_{S_a}+\phi_{S_b}) + A_{TT}^{\cos(4\phi-\phi_{S_a}-\phi_{S_b})} \cos(4\phi-\phi_{S_a}-\phi_{S_b}) \\
&+ A_{TT}^{\cos(2\phi-\phi_{S_a}+\phi_{S_b})} \cos(2\phi-\phi_{S_a}+\phi_{S_b}) + A_{TT}^{\cos(2\phi+\phi_{S_a}-\phi_{S_b})} \cos(2\phi+\phi_{S_a}-\phi_{S_b}) \Big)\Big] \qquad (2.1.10)
\end{aligned}
$$

4. In the q_T-dependent cross section, all the chiral-odd parton distributions disappear after integrating over the azimuthal angle ϕ. On the other hand, all the chiral-even effects survive this integration.

5. The large number of independent SFs to be determined from the polarized DY processes at NICA (24 for identical hadrons in the initial state) is sufficient to map out all eight leading twist TMD PDFs for quarks and anti-quarks. This fact indicates the high potential of the polarized DY process for studying new PDFs. This process has also a certain advantage over SIDIS [10, 11] which also capable of mapping out the leading twist TMD PDFs but requires knowledge of fragmentation functions.

6. The transverse single spin asymmetries depending on the Structure Functions F_{UT}^{1} or F_{TU}^{1} are of the particular interests. The both SFs contain the Sivers PDF which was predicted to have the opposite sign in DY as compared to SIDIS [12, 13, 14]. As the sign reversal is at the core of our present understanding of transverse single spin asymmetries in hard scattering processes, the experimental check of this prediction is of the utmost importance.

7. The expected sign reversal of T-odd TMDs can also be investigated through the structure functions $F_{TU}^{\sin(2\phi-\phi_a)}$ or $F_{UT}^{\sin(2\phi-\phi_b)}$ in which the Boer-Mulders PDF enters (see [15, 16, 17]).
8. It is very important to measure those new TMD PDFs which are still not measured or measured with large uncertainties. These are worm-gear-T, L and pretzelosity PDFs. The last one would give new information on possible role of the constituent's orbital momenta in resolution of the nucleon spin crisis.
9. For the complete success of the nucleon structure study program it is mandatory that NICA provides beams of all above mentioned configurations (see also Section 3). The expected effects are of the order of a few percent. So the high luminosity, $\geq 10^{32}$, is necessary to guaranty a corresponding statistical accuracy of measurements.
10. As usual, the new facility, i.e. NICA and SPD, prior to measurements of something unknown, should show its potentials measuring already known quantities. So, the program of the nucleon structure study at NICA should start with measurements of non-polarized SFs. Measuring σ^{00}_{int} (Eq. 2.1.9) we could obtain the structure function F^{1}_{UU} which is proportional to the PDF f_1 (Eq.2.1.5) – quite well measured in SIDIS experiments. Additionally from measurements of A_{UU} (Eq. 2.1.10) we obtain $F^{cos2\phi}_{UU}$ which is proportional to the Boer-Mulders PDF and still poor measured.
11. Next step in the program should be measurements of the A_{LL} asymmetry which provide the access to the SFs F^{1}_{LL} and $F^{cos2\phi}$ .The first one is proportional to the helicity PDF, well measured in SIDIS, while the second one is proportional to the still unknown worm-gear-L PDF.

2.1.2. Studies of PDFs via integrated asymmetries.

The set of asymmetries (2.1.10) gives the access to all eight leading twist TMD PDFs. However, sometimes one can work with integrated asymmetries. Integrated asymmetries are useful for the express analysis of data and checks of expected relations between asymmetries mentioned in Section 2.1. They are also useful for model estimations and determination of required statistics (see Section 6.2). Let us consider several examples starting from the case when only one of colliding hadrons (for instance, hadron "b") is transversely polarized. In this case the DY cross section Eq. (2.1.2) with SFs given by Eq. (2.1.6) is reduced to the expression (2.1.11) which, being integrated over ϕ_{Sb}, allows to construct the weighted asymmetries given by Eqs. (2.1.12) where $\phi_{S_b} \equiv \phi_S$ (the weight function is shown in the superscript of the asymmetry). They provide access to the Boer-Mulders, Sivers, and pretzelosity TMD PDFs. The integrated and additionally q_T -weighted asymmetries $A_{UT}^{w\left[\sin(\phi+\phi_S)\frac{q_T}{M_N}\right]}$ and $A_{UT}^{w\left[\sin(\phi-\phi_S)\frac{q_T}{M_N}\right]}$ given by Eqs. (2.1.13-14) provide access to the first moments of the Boer-Mulders, $h_{1q}^{\perp}(x,k_T^2)$, and Sivers , $f_{q1T}^{\perp(1)}(x,k_T^2)$, PDFs given by Eqs. (2.1.15).

$$
\begin{aligned}
\frac{d\sigma}{dx_a dx_b d^2\mathbf{q}_T d\Omega} = \frac{\alpha^2}{4Q^2}\Bigg\{ & (1+\cos^2\theta)\; C\left[f_1 \bar{f}_1 \right] \\
& +\sin^2\theta\cos 2\phi\; C\left[\frac{2(\vec{h}\cdot\vec{k}_{aT})(\vec{h}\cdot\vec{k}_{bT}) - \vec{k}_{aT}\cdot\vec{k}_{bT}}{M_a M_b} h_1^{\perp}\bar{h}_1^{\perp} \right] \\
& +|S_{bT}|\Bigg[(1+\cos^2\theta)\sin(\phi-\phi_{S_b})\; C\left[\frac{\vec{h}\cdot\vec{k}_{bT}}{M_b} f_1 \bar{f}_{1T}^{\perp} \right] - \sin^2\theta\sin(\phi+\phi_{S_b})\; C\left[\frac{\vec{h}\cdot\vec{k}_{aT}}{M_a} h_1^{\perp}\bar{h}_1 \right] \\
& -\sin^2\theta\sin(3\phi-\phi_{S_b})\; C\left[\frac{2(\vec{h}\cdot\vec{k}_{bT})[2(\vec{h}\cdot\vec{k}_{aT})(\vec{h}\cdot\vec{k}_{bT}) - \vec{k}_{aT}\cdot\vec{k}_{bT}] - \vec{k}_{bT}^2(\vec{h}\cdot\vec{k}_{aT})}{2M_a M_b^2} h_1^{\perp}\bar{h}_{1T}^{\perp} \right] \Bigg] \Bigg\},
\end{aligned} \tag{2.1.11}
$$

For the *pp* collisions there are two limiting cases when one can neglect contributions to the asymmetries from sea part of PDFs either of polarized or non-polarized protons. The first case corresponds to the region of x_{Bj} values where $x_{unpol} >> x_{pol}$ while the second one-- to the region $x_{unpol} << x_{pol}$. In these cases one can obtain the approximate expressions for asymmetries (2.1.13-14) which are given by Eqs. (2.1.16-17)

So far we have considered the pp collisions. At NICA we are planning to study the pd and dd collisions as well. As is known from COMPASS experiment, the SIDIS asymmetries on polarized deuterons are consisted with zero. At NICA we can expect that asymmetries $A_{UT}^{w\left[\sin(\phi\pm\phi_S)\frac{q_T}{M_N}\right]}\Big|_{pD^{\uparrow}}$, $A_{UT}^{w\left[\sin(\phi\pm\phi_S)\frac{q_T}{M_N}\right]}\Big|_{DD^{\uparrow}}$ also will be consisted with zero (subject of tests).

But asymmetries in $Dp\uparrow$ collisions are expected to be non-zero. In the limiting cases $x_D >> x_{p^\uparrow}$ and $x_D << x_{p^\uparrow}$ these asymmetries (**accessible only at NICA**) are given by expressions (2.1.18).

$$A_{UT}^{w[\sin(\phi+\phi_S)]} = \frac{\int d\Omega\, d\phi_S \sin(\phi+\phi_S)\left[d\sigma^{\uparrow} - d\sigma^{\downarrow}\right]}{\int d\Omega d\phi_S\left[d\sigma^{\uparrow} + d\sigma^{\downarrow}\right]/2} = -\frac{1}{2}\frac{C\left[\frac{\vec{h}\cdot\vec{k}_{aT}}{M_a} h_1^{\perp}\bar{h}_1\right]}{C\left[f_1\bar{f}_1\right]},$$

$$A_{UT}^{w[\sin(\phi-\phi_S)]} = \frac{\int d\Omega\, d\phi_S \sin(\phi-\phi_S)\left[d\sigma^{\uparrow} - d\sigma^{\downarrow}\right]}{\int d\Omega d\phi_S\left[d\sigma^{\uparrow} + d\sigma^{\downarrow}\right]/2} = \frac{1}{2}\frac{C\left[\frac{\vec{h}\cdot\vec{k}_{bT}}{M_b} f_1\bar{f}_{1T}^{\perp}\right]}{C\left[f_1\bar{f}_1\right]}, \qquad (2.1.12)$$

$$A_{UT}^{w[\sin(3\phi-\phi_S)]} = \frac{\int d\Omega\, d\phi_S \sin(3\phi-\phi_S)\left[d\sigma^{\uparrow} - d\sigma^{\downarrow}\right]}{\int d\Omega d\phi_S\left[d\sigma^{\uparrow} + d\sigma^{\downarrow}\right]/2} =$$

$$= -\frac{1}{2}\frac{C\left[\frac{2(\vec{h}\cdot\vec{k}_{bT})[2(\vec{h}\cdot\vec{k}_{aT})(\vec{h}\cdot\vec{k}_{bT}) - \vec{k}_{aT}\cdot\vec{k}_{bT}] - \vec{k}_{bT}^2(\vec{h}\cdot\vec{k}_{aT})}{2M_a M_b^2} h_1^{\perp}\bar{h}_{1T}^{\perp}\right]}{C\left[f_1\bar{f}_1\right]},$$

$$A_{UT}^{w\left[\sin(\phi+\phi_S)\frac{q_T}{M_N}\right]} = \frac{\int d\Omega\int d^2\mathbf{q}_T(|\mathbf{q}_T|/M_p)\sin(\phi+\phi_S)\left[d\sigma^{\uparrow} - d\sigma^{\downarrow}\right]}{\int d\Omega\int d^2\mathbf{q}_T\left[d\sigma^{\uparrow} + d\sigma^{\downarrow}\right]/2}$$

$$= -\frac{\sum_q e_q^2\left[\bar{h}_{1q}^{\perp(1)}(x_p)h_{1q}(x_{p\uparrow}) + (q\leftrightarrow\bar{q})\right]}{\sum_q e_q^2\left[\bar{f}_{1q}(x_p)f_{1q}(x_{p\uparrow}) + (q\leftrightarrow\bar{q})\right]}, \qquad (2.1.13)$$

$$A_{UT}^{w\left[\sin(\phi-\phi_S)\frac{q_T}{M_N}\right]} = \frac{\int d\Omega\int d^2\mathbf{q}_T(|\mathbf{q}_T|/M_p)\sin(\phi-\phi_S)\left[d\sigma^{\uparrow} - d\sigma^{\downarrow}\right]}{\int d\Omega\int d^2\mathbf{q}_T\left[d\sigma^{\uparrow} + d\sigma^{\downarrow}\right]/2}$$

$$= 2\frac{\sum_q e_q^2\left[f_{1T}^{\perp(1)q}(x_{p\uparrow})\bar{f}_{1q}(x_p) + (q\leftrightarrow\bar{q})\right]}{\sum_q e_q^2\left[\bar{f}_{1q}(x_{p\uparrow})f_{1q}(x_p) + (q\leftrightarrow\bar{q})\right]}, \qquad (2.1.14)$$

where

$$h_{1q}^{\perp(1)}(x) = \int d^2k_T \left(\frac{k_T^2}{2M_p^2}\right) h_{1q}^{\perp}(x_p,k_T^2) \quad ; \quad f_{q1T}^{\perp(1)}(x) = \int d^2k_T \left(\frac{k_T^2}{2M_p^2}\right) f_{q1T}^{\perp(1)}(x,k_T^2). \quad (2.1.15)$$

$$A_{UT}^{w\left[\sin(\phi-\phi_S)\frac{q_T}{M_N}\right]}\Bigg|_{x_p>>x_{p\uparrow}} \approx 2\frac{\bar{f}_{1uT}^{\perp(1)}(x_{p\uparrow})}{\bar{f}_{1u}(x_{p\uparrow})} \quad ; \quad A_{UT}^{w\left[\sin(\phi+\phi_S)\frac{q_T}{M_N}\right]}\Bigg|_{x_p>>x_{p\uparrow}} \approx -\frac{h_{1u}^{\perp(1)}(x_p)\bar{h}_{1u}(x_{p\uparrow})}{f_{1u}(x_p)\bar{f}_{1u}(x_{p\uparrow})} \quad (2.1.16)$$

$$A_{UT}^{w\left[\sin(\phi-\phi_S)\frac{q_T}{M_N}\right]}\Bigg|_{x_p<<x_{p\uparrow}} \approx 2\frac{f_{1uT}^{\perp(1)}(x_{p\uparrow})}{f_{1u}^{\perp(1)}(x_{p\uparrow})} \quad ; \quad A_{UT}^{w\left[\sin(\phi+\phi_S)\frac{q_T}{M_N}\right]}\Bigg|_{x_p<<x_{p\uparrow}} \approx -\frac{\bar{h}_{1u}^{\perp(1)}(x_p)h_{1u}(x_{p\uparrow})}{\bar{f}_{1u}(x_p)f_{1u}(x_{p\uparrow})}. \quad (2.1.17)$$

$$A_{UT}^{w\left[\sin(\phi-\phi_S)\frac{q_T}{M_N}\right]}(x_D>>x_{p\uparrow})\Bigg|_{Dp\uparrow\to l^+l^-X} \approx \frac{4\bar{f}_{1uT}^{\perp(1)}(x_{p\uparrow})+\bar{f}_{1dT}^{\perp(1)}(x_{p\uparrow})}{4\bar{f}_{1u}^{\perp(1)}(x_{p\uparrow})+\bar{f}_{1d}^{\perp(1)}(x_{p\uparrow})},$$

$$A_{UT}^{w\left[\sin(\phi-\phi_S)\frac{q_T}{M_N}\right]}(x_D<<x_{p\uparrow})\Bigg|_{Dp\uparrow\to l^+l^-X} \approx 2\frac{4f_{1uT}^{\perp(1)}(x_{p\uparrow})+f_{1dT}^{\perp(1)}(x_{p\uparrow})}{4f_{1u}^{\perp(1)}(x_{p\uparrow})+f_{1d}^{\perp(1)}(x_{p\uparrow})},$$

(2.1.18)

$$A_{UT}^{w\left[\sin(\phi+\phi_S)\frac{q_T}{M_N}\right]}(x_D>>x_{p\uparrow})\Bigg|_{Dp\uparrow\to l^+l^-X} \approx -\frac{[h_{1u}^{\perp(1)}(x_D)+h_{1d}^{\perp(1)}(x_D)][4\bar{h}_{1u}(x_{p\uparrow})+\bar{h}_{1d}(x_{p\uparrow})]}{[f_{1u}(x_D)+f_{1d}(x_D)][4\bar{f}_{1u}(x_{p\uparrow})+\bar{f}_{1d}(x_{p\uparrow})]},$$

$$A_{UT}^{w\left[\sin(\phi+\phi_S)\frac{q_T}{M_N}\right]}(x_D<<x_{p\uparrow})\Bigg|_{Dp\uparrow\to l^+l^-X} \approx -\frac{[\bar{h}_{1u}^{\perp(1)}(x_D)+\bar{h}_{1d}^{\perp(1)}(x_D)][4h_{1u}(x_{p\uparrow})+h_{1d}(x_{p\uparrow})]}{[\bar{f}_{1u}(x_D)+\bar{f}_{1d}(x_D)][4f_{1u}(x_{p\uparrow})+f_{1d}(x_{p\uparrow})]}.$$

In case of double transversely polarized hadrons, instead of complicated analysis of the A_{TT} asymmetry given by Eq. (2.1.10), the direct access to the transversity PDF h_1 one can have via the weighted asymmetry, $A^{w[\cos(\phi_{Sb}+\phi_{Sa})\,q_T/M]}$, integrated over the angles ϕ_{Sb} and ϕ_{Sa} :

$$A_{TT}^{w[\cos(\phi_{Sb}+\phi_{Sa})q_T/M]} \equiv A_{TT}^{\text{int}} = \frac{\sum_q e_q^2\left(\bar{h}_{1q}(x_1)h_{1q}(x_2)+(x_1\leftrightarrow x_2)\right)}{\sum_q e_q^2\left(\bar{f}_{1q}(x_1)f_{1q}(x_2)+(x_1\leftrightarrow x_2)\right)}. \quad (2.1.19)$$

The method of integrated asymmetries requires calculations of corresponding cross sections prior their integration. It means that the detector acceptance and luminosity should be under control.

2.2. New nucleon PDFs and *J/Ψ* production mechanisms. (**TO BE UPDATED**)

The *J/Ψ* meson, a bound state of charm and anti-charm quarks, was discovered in 1974 at BNL [18] and SLAC [19]. The production and binding mechanisms of these two quarks are still not completely known. It is important to note that many of *J/Ψ* mesons observed so far are not directly produced from collisions but are the result of decays of other charmonium states. Recently it has been estimated that 30 ± 10 % of *J/Ψ* mesons come from χ_c decays, and 59 ±10 % of them are produced directly [20]. The *J/Ψ* production mechanism, included in the PYTHIA simulation code and intended for collider applications, considers two approaches: “colour singlet” and “colour octet” ones. The “colour singlet” approach considers *gg* fusion processes, while “colour octet” considers *gg*, *gq* and *qq* processes. According to PYTHIA [21], in *pp* collisions at √s=24 GeV the cross section of the *J/Ψ* production in *gg* processes (singlet and octet) and in *gq* plus *qq* processes are about equal (~53 and ~50 nb, respectively). The *gq* and *qq* processes proceed via various charmonium states subsequently decaying into *J/Ψ*. So, these processes could be sensitive to the TMD PDFs. It is interesting to note that the *gq-bar* processes have the largest cross sections (see the Table 1 in Appendix 1).

The production of *J/Ψ* with it subsequent decay into a lepton pair, proceeding via the $q\bar{q}$ - or $g\bar{q}$ processes, $H_a + H_b \rightarrow J/\Psi + X \rightarrow l^+ + l^- + X$, , is analogous to the DY production mechanism (Eq. 2.1.1) if the *J/Ψ* interaction with quarks and leptons is of the vector type. This analogy is known under the name “duality model” [22, 23]. In the case of the TMD PDFs studies, the “duality model” can predict [24] a similar behavior of asymmetries $A^i_{jk} = F^i_{jk}/F^1_{UU}$ in the lepton pair’s production calculated via DY (Eq. 2.1.10) and via *J/Ψ* events. This similarity follows from the duality model idea to replace the coupling e_q^2 in the convolutions for F^i_{jk} (Eq.2.1.4) by *J/Ψ* vector coupling with $q\bar{q}$ $(g_q^V)^2$. The vector couplings are expected to be the same for *u* and *d* quarks [22] and cancel in the ratios $A^i_{jk} = F^i_{jk}/F^1_{UU}$ for large x_a or x_b. For instance, we can compare the Sivers asymmetry $A_{UT}^{w\left[\sin(\phi-\phi_S)\frac{q_T}{M_N}\right]}$ given in the DY case by Eq. (2.1.14) with the same asymmetry given in *J/Ψ* case by Eq. (2.1.14) with omitted quark charges. At NICA such a comparison can be performed at various colliding beam energies.

2.3. Direct photons.

Direct photon productions in the non-polarized and polarized *pp (pd)* reactions provide information on the gluon distributions in nucleons (Fig. 2.3). There are two main hard processes where direct photons can be produced: gluon Compton scattering, *g+q→γ+X*, and quark-antiquark annihilation, *q+ qbar →γ+X*. As it has been pointed out in [25], “the direct photon production in non polarized *pp* collisions can provide a clear test of short-distance dynamics as predicted by the perturbative QCD, because the photon originates in the hard scattering sub-process and does not fragment. This immediately means that Collins effect is not present. The process is very sensitive to the non polarized gluon structure function, since it is dominated by quark-gluon Compton sub process in a large photon transverse momentum range”.

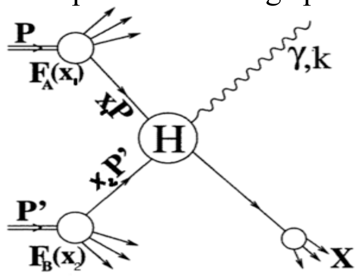

Fig.2.3: *diagram of the direct photon production. Vertex H corresponds to q + qbar →γ+g or g+q→γ+q hard processes.*

The non- polarized cross section for production of a photon with the transverse momentum p_T and rapidity *y* in the reaction $p+p\rightarrow \gamma+X$ is written [25] as follows:

$$d\sigma = \sum_i \int_{x_{min}}^{1} dx_a \int d^2\mathbf{k}_{Ta} d^2\mathbf{k}_{Tb} \frac{x_a x_b}{x_a - (p_T/\sqrt{s})e^y} \left[q_i(x_a, \mathbf{k}_{Ta}) G(x_b, \mathbf{k}_{Tb}) \times \frac{d\hat{\sigma}}{d\hat{t}}(q_i G \to q_i \gamma) + G(x_a, \mathbf{k}_{Ta})\, q_i(x_b, \mathbf{k}_{Tb}) \frac{d\hat{\sigma}}{d\hat{t}}(G q_i \to q_i \gamma) \right],$$

where k_{Ta} (k_{Tb}) is the transverse momentum of the interacting quark (gluon), x_a (x_b) is the fraction of the proton momentum carried by them and $q_i(x, k_T)$, [$G(x, k_T)$] is the quark (gluon) distribution function with the specified k_T [25]. The total cross section of the direct photon production in the *pp*-collision at $\sqrt{s}$=24 GeV via the first process (according to PYTHIA 6.4) is equal to1100 nbn, while the cross section of the second process is about 200 nbn. So, the gluon Compton scattering is the main mechanism of the direct photon production. One can show [25], that the above expression can be used also for extraction of the polarized gluon distribution (Sivers gluon function) from measurement of the transverse single spin asymmetry A_N defined as follows:

$$A_N = \frac{\sigma^{\uparrow} - \sigma^{\downarrow}}{\sigma^{\uparrow} + \sigma^{\downarrow}}$$

Here $\sigma\uparrow$ and $\sigma\downarrow$ are the cross sections of the direct photon production for the opposite transverse polarizations of one of the colliding protons. In [26] it has been pointed out that the asymmetry A_N at large positive x_F is dominated by quark-gluon correlations while at large negative x_F [27] it is dominated by pure gluon-gluon correlations. The further development of the corresponding formalism can be found in [28], [29].

Predictions for the value of A_N at $\sqrt{s}$=30 GeV, p_T=4 GeV/c can be found in [28] for negative x_F (Fig. 2.4 (left)) and in [26] for positive x_F (Fig. 2.4 (right)). In both cases the A_N values remain sizable.

The first attempt to measure A_N at $\sqrt{s}$=19.4 GeV was performed in the fixed target experiment E704 at Fermilab [30] in the kinematic range $-0.15<x_F<0.15$ and $2.5<p_T<3.1$ GeV/c. Results are consistent with zero within large statistical and systematic uncertainties (Fig.2.5).

The single spin asymmetries in the direct photon production will be measured also by PHENIX [31] and STAR [32] at RHIC.

Production of direct photons at large transverse momentum with longitudinally polarized proton beams is a very promising method to measure gluon polarization Δg [33]. Longitudinal double spin asymmetry A_{LL}, defined as:

$$A_{LL} = \frac{(\sigma_{++} + \sigma_{--}) - (\sigma_{+-} + \sigma_{-+})}{(\sigma_{++} + \sigma_{--}) + (\sigma_{+-} + \sigma_{-+})}$$

where $\sigma_{\pm\pm}$ are cross sections for all four helicity combinations, can be written (assuming dominance of the Compton process) as [34]:

$$A_{LL} \approx \frac{\Delta g(x_1)}{g(x_1)} \cdot \left[\frac{\sum_q e_q^2 \left[\Delta q(x_2) + \Delta\bar{q}(x_2)\right]}{\sum_q e_q^2 \left[q(x_2) + \bar{q}(x_2)\right]} \right] \cdot \hat{a}_{LL}(gq \to \gamma q) + (1 \leftrightarrow 2),$$

where the second factor is known as A_1^p asymmetry (Section 1.1) from polarized SIDIS and $a_{LL}(gq\to\gamma q)$ is spin asymmetry for sub-process $gq\to\gamma q$.

Measurement of A_{LL} at $\sqrt{s}$>100 GeV is included in the long range program of RHIC [34].

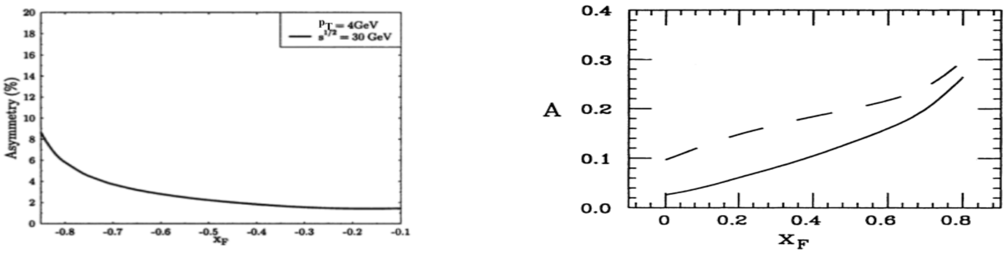

Fig. 2.4: *predictions for A_N at $\sqrt{s}$=30 GeV, p_T=4 GeV/c: from [28](left), from [26] (right).*

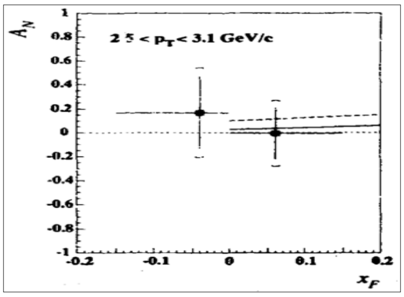

***Fig.2.5*:** the single transverse spin asymmetry A_N measured in the E704 experiment. Curves are predictions of [26].

Sections 2.4 – 2.6 to be updated.

2.6. Spin-dependent reactions in heavy ion collisions. (to be updated)

*2.6.1. Proposal for the birefringence phenomenon investigation at NICA facility***.**

One of the most interesting quasi-optical effects – the birefringence phenomenon for deuterons (or other particles with spin S ≥ 1) passing through matter – has recently become the area of research [35]. Birefringence occurs when spin S ≥ 1 particles pass through isotropic non-polarized matter and is due to the inherent anisotropy of particles with spin S ≥ 1 (as distinct from spin ½ particles). The birefringence effect leads to the rotation of the beam polarization vector when a non-polarized deuteron beam passes through a non-polarized target. Moreover, the appearing spin dichroism effect (the different absorption of deuterons in states with m = ±1 and 0) gives rise to a tensor polarization of the initially non-polarized deuteron beam that has passed through the non-polarized target [35]. It is noteworthy that the rotation angle of the polarization vector and the spin dichroism are determined by the real and imaginary parts of the amplitude of zero-angle coherent elastic scattering, respectively. For this reason it is possible to measure these amplitudes in experiments.

The experimental investigation of the birefringence effect began with the observation of the spin dichroism effect for low- and high-energy deuterons. The experiments with 5-20 MeV deuterons were performed on the electrostatic accelerator at Cologne University (Germany) [36]. Tensor polarization acquired by the beam was obtained by varying the thickness of carbon targets and the initial energy of the beam.

The experiments using carbon targets and deuterons with a momentum of 5GeV/c were performed at «Nuclotron-M» accelerator. The measured values of tensor polarization acquired by the beam passing through a set of variable-thickness targets are given in Fig.2.6 [37].

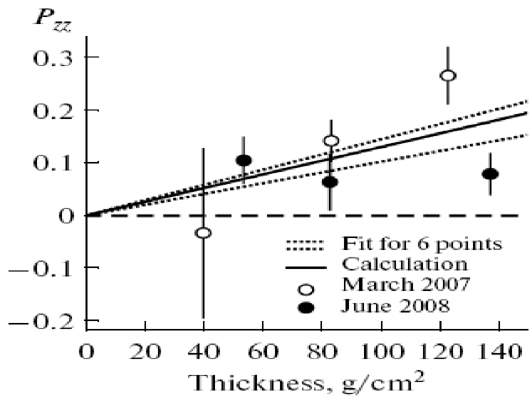

Fig.2.6: *tensor polarization value acquired by deuterons of 5 GeV/c crossing the carbon target of various thickness.*

Based on the performed theoretical and experimental studies, we can highlight the following directions for future research in fixed target and collider experiments of the NICA complex:

1. The study of birefringence (spin rotation, spin dichroism) in few-nucleon systems involving protons and deuterons.

2. The study of birefringence appearing through the interaction of protons or deuterons with heavy nuclei.

3. The study of birefringence for heavy nuclei with spin $S \geq 1$.

4. The study of the birefringence effect in the nuclear matter of vector particles produced in inelastic collisions.

2.7. Future experiments on nucleon structure in the world. (to be updated)

The measurements of DY processes using various beams and targets have started in 1970 with the unpolarized proton beam of AGS accelerator in Brookhaven. Since that time series of DY experiments were performed at FNAL and CERN but only two of them directly connected with studies of the nucleon structure. These are experiments NA51 [38] and E866 [39]. Both of them have measured the ratio of the anti-d and anti-u quarks in the nucleons.

Present list of the DY experiment in the world (Table below) includes fixed target and collider experiments aimed to study spin-dependent and spin-independent processes in a wide range of energies. Physics goals of the experiments include studies of one or several TMD PDFs.

The first fixed target polarized DY measurements will be performed at CERN by the COMPASS-II experiment [40]. It will start the data taking in 2014 with 160 GeV (or $\sqrt{s} \sim$ 18GeV) π^- beam and polarized hydrogen target. The FNAL E-906 [41]non-polarized experiment has started already. Recently FNAL has initiated the workshops on polarized DY experiments. The PANDA [42]at FAIR will start somewhat later.

Future collider DY experiments are included in the long range programs of the PHENIX and STAR at RHIC [43]. They are planning to carry out DY measurements with 500 GeV longitudinally polarized as well as with 200 GeV transversely polarized protons.

The Spin Physics Detector (SPD) experiments, proposed at the second interaction point of the NICA collider, will have a number of advantages for DY measurements related to nucleon structure studies. These advantages include:

- operations with *pp, pd and dd* beams,
- scan of effects on beam energies,
- measurement of effects via muon and electron-positron pairs simultaneously,
- operations with non-polarized, transversely and longitudinally polarized beams or their combinations. Such possibilities permit for **the first time** to perform comprehensive studies of **all leading twist PDFs** of nucleons in a single experiment with minimal systematic errors.

Experiment	**CERN, COMPASS**	**FAIR, PANDA**	**FNAL, E-906**	**RHIC, STAR**	**RHIC-PHENIX**	**NICA, SPD**
mode	*fixed target*	*fixed target*	*fixed target*	*collider*	*collider*	*collider*
Beam/target	*π-, p*	*anti-p, p*	*π-, p*	*pp*	*pp*	*pp, pd,dd*
Polarization:b/t	*0; 0.8*	*0; 0*	*0; 0*	*0.5*	*0.5*	*0.5*
Luminosity	10^{32}	10^{32}	10^{42}	10^{32}	10^{32}	10^{32}
√s , GeV	*17*	*6*	*16*	*200, 500*	*200, 500*	*10-26*
$x_{1(beam)}$ *range*	*0.1-1.0*	*0.1-1.0*	*0.1-1.0*	*0.1-0.9*	*0.1-0.9*	*0.1-0.8*
q_T*, GeV*	*0.5 -4.0*	*0.5 -1.5*	*0.5 -3.0*	*1.0 -10.0*	*1.0 -10.0*	*0.5 -6.0*
Lepton pairs,	*μ-μ+*	*μ-μ+*	*μ-μ+*	*μ-μ+*	*μ-μ+*	*μ-μ+, e+e-*
Data taking	*2014*	*>2016*	*2013*	*>2016*	*>2016*	*>2017*
Transversity	**YES**	**NO**	**NO**	**YES**	**YES**	**YES**

Boer-Mulders	**YES**	**YES**	**YES**	**YES**	**YES**	**YES**
Sivers	**YES**	**YES**	**YES**	**YES**	**YES**	**YES**
Pretzelosity	**YES**	**NO**	**NO**	**NO**	**YES**	**YES**
Worm Gear	**YES**	**NO**	**NO**	**NO**	**NO**	**YES**
J/Ψ	**YES**	**YES**	**NO**	**NO**	**NO**	**YES**
Flavour separ	**NO**	**NO**	**YES**	**NO**	**NO**	**YES**

3. Requirements to the NUCLOTRON-NICA complex

The research program outlined in Section 2 requires definite characteristics of beams and technical infrastructure.

Beams. The following beams will be needed, polarized and non-polarized:

$$pp,\ pd,\ dd,\ pp^{\uparrow},\ pd^{\uparrow},\ p^{\uparrow}p^{\uparrow},\ p^{\uparrow}d^{\uparrow},\ d^{\uparrow}d^{\uparrow}.$$

Beam polarizations both at MPD and SPD: longitudinal and transversal. Absolute values of polarizations should be ≥ 50%.The life time of the beam polarization should be long enough, ≥24h. Measurements of Single Spin and Double Spin asymmetries in *DY* require running in different beam polarization modes: *UU, LU, UL,TU, UT,LL ,LT and TL* (spin flipping for every bunch or group of bunches should be considered).

Beam energies: $p^{\uparrow}p^{\uparrow}(\sqrt{s_{pp}}) = 12 \div \geq 27$ GeV ($5 \div \geq 12.6$ GeV kinetic energy),

$d^{\uparrow}d^{\uparrow}(\sqrt{s_{NN}}) = 4 \div \geq 13.8$ GeV ($2 \div \geq 5.9$ GeV/u ion kinetic energy).

Asymmetric beam energies should be considered also.

Beam luminosities: in the *pp* mode: $L_{average} \geq 1\cdot 10^{32}$ cm^{-2}s^{-1} (at $\sqrt{s_{pp}} = 27$ GeV),

in the *dd* mode: $L_{average} \geq 1\cdot 10^{30}$ cm^{-2}s^{-1} (at $\sqrt{s_{NN}} = 14$ GeV).

For estimations of the expected statistics of events, we assume that total efficiency of the NICA complex will be ≥ 80%, i.e. total working hours per year will be ≥ 7000 hours.

Infrastructure. The infrastructure of the Nuclotron-NICA complex should include:

- a source(s) of polarized (non-polarized) protons and deuterons,
- a system of polarization control and absolute measurements (3-5%),
- a system of luminosity control and absolute measurements,
- a system(s) of data distribution on polarization and luminosity to the experiments.

The infrastructure tasks should be subjects of the separate project(s).

Local SPD polarization and luminosity monitors are discussed in Section 5.6.

Beams intersection area. The area of ± 3m along and across of the beams second intersection point, where the detector for the spin physics experiment will be situated, must be free of any collider elements and equipment. The beam pipe diameter in this region should be minimal, 10 cm or less, to guaranty the angular detector acceptance close to 4π. The walls of the beam pipe in the region ± 1m of the beams intersections should have a minimal thickness and made of the low-Z material (Be?).

4. Polarized beams at NICA. (TO BE UPDATED)

The NICA complex at JINR has been approved in 2008 assuming two phases of the construction. The first phase being realized now includes construction of facilities for heavy ion physics program [1] while the second phase should include facilities for the program of spin physics studies with polarized protons and deuterons. In this document we communicate briefly the status of the NICA project in relation to research with polarized beams.

4.1. Scheme of the complex.

The main elements of NICA complex are shown in Figure 4.1. They include: the heavy ion source and source of polarized ions (proton and deuteron), SPI, with corresponding linacs,

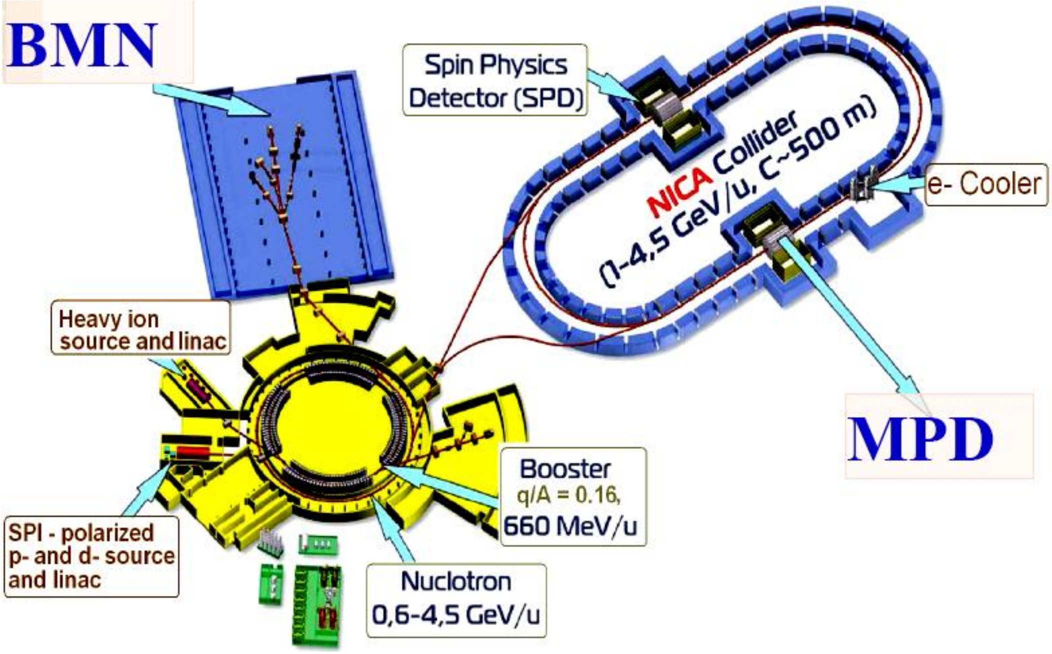

***Fig. 4.1:** The NICA complex of JINR.*

existing superconducting accelerator Nuclotron upgraded to Nuclotron M, new superconducting Booster synchrotron , new collider NICA with two detectors – MPD (Multi-Purpose Detector for heavy ion studies) and SPD (Spin Physics Detector), as well as experimental hall for fixed target experiments with beams extracted from Nuclotron M.

The functional scheme of facility approved for the first phase of construction scenario is presented in Fig.4.2. The chain of beams injection to the collider rings in the case of polarized protons and deuterons includes: SPI, the modernized injection linac LU-20 equipped with the new pre-injector (PI), (Booster), Nuclotron , NICA. The main goals of the Booster in polarized case are the following: 1) formation of the required beam emittance with electron cooling and 2) fast extraction of the accelerated beam. The chain bypassing Booster is also considered [2].

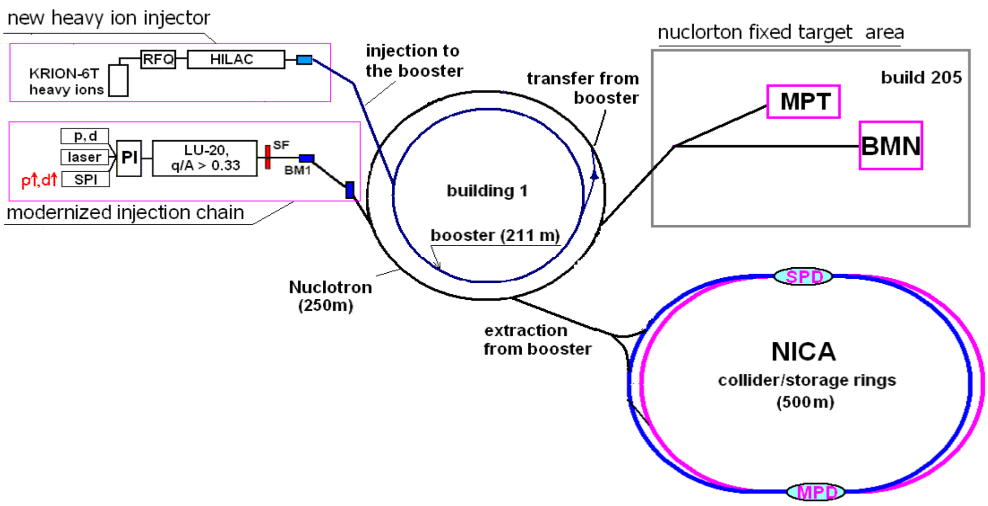

***Fig. 4.2:** The functional scheme of NICA complex.*

Feasibilities to fulfill requirements to the NICA complex formulated in previous Section are considered below moving along the chain: SPI – LU-20 – Nuclotron (Booster) – NICA.

4.2. Source of polarized ions and injector.

The new polarized ion source is being commissioned now. It was designed and constructed as a universal pulsed high intensity source of polarized deuterons and protons based on a charge-exchange plasma ionizer. The output ↑D^+ (↑H^+) current of the source is expected to be at a level of 10 mA. The expected polarization is about 90% in the vector (±1) for ↑D^+ and ↑H^+ and tensor (+1,−2) for ↑D^+ modes. The project is carried out in cooperation with INR of RAS (Moscow). The equipment available from the CIPIOS ion source (IUCF, Bloomington, USA) is partially used for SPI. The source will deliver the 10 mks pulsed polarized proton or deuteron beam with intensity up to ~$2 \cdot 10^{11}$ per pulse and repetition rate of 1 Hz [3].

Briefly, the SPI consists of several sections. The atomic section uses the permanent (B = 1.4 T) and conventional electromagnet sextupoles (B = 0.9 T) for beam focusing. The cryocooler section is used for cooling the atomic beam. In the radio-frequency transition section the atoms are polarized before they are focused into the ionizer. The resonant charge-exchange ionizer [4] produces pulses of positive ion plasma inside the solenoid. Nearly resonant charge-exchange reactions:

$$D^+ + H^0\uparrow \; \rightarrow H^+\uparrow + D^0 \,, \qquad (1)$$

$$H^+ + D^0\uparrow \; \rightarrow D^+\uparrow + H^0 \,, \qquad (2)$$

are used to produce polarized protons or deuterons. Spin orientation of ↑D^+ (↑H^+) at the exit of SPI is vertical. The polarized particles are focused through the extraction section into the injection linac.

The Alvarez-type linac LU-20 used as the Nuclotron injector was put into operation in 1974. It was originally designed as proton accelerator from 600 KeV to 20 MeV. Later it was modified to accelerate ions with charge-to-mass ratio q/A > 0.33 to 5 MeV/u at 2βλ mode. The pulse transformer voltage up to 700 kV is now used to feed the accelerating tube of the LU-20 pre-injector. The new pre-injector will be based on the RFQ section [5].

4.3. Acceleration of polarized protons and deuterons at Nuclotron.

4.3.1. Polarized deuterons.

Acceleration of polarized deuterons at the Synchrophasotron was achived for the first time in 1984 [6] and at Nuclotron in 2002 [7]. There are no dengerous spin resonances wich could occure during the polarized deuterons acceleration in Nuclotron up to the energy of 5.6 GeV/u. This limit is practically very close to the maximum design energy of the Nuclotron (6 GeV/u for q/A = ½). There are no doubts about the realization of the project in this case. The only problem in case of deuterons is changing the polarization direction from vertical to horizontal and back.

4.3.2. Polarized protons.

According to the NICA project, Nuclotron as the strong focusing synchrotron should accelerate polarized protons from the injection energy (20 MeV) up to the maximum design value of 12.6 GeV. Let us estimate first the expected proton beam intensity at the Nuclotron output. The limitations and particle losses could come due to different reasons. Taking the SPI design current (10 mA) and estimated particle loss coefficient between the source and Nuclotron (0.5), RF capture (0.8), extraction efficiency (0.86) and other factors in the synchrotron (0.9), one can expect the output intensity up to $1.6 \cdot 10^{11}$ polarized protons per pulse.

For the successful crossing of numerous spin resonances in Nuclotron, the inserted devices like "siberian snakes" will be designed and installed into the accelerator lattice. Spin resonanses, occuring during the acceleration cycle at different combinations of the betatron (ν_x , ν_y) and spin (ν) oscillation frequencies, were analyzed in [8].Three cases were considered: $\nu = k$, $\nu = k \pm \nu_y$, $\nu = k \pm \nu_x$, where k = 0, 1, 2,.. . Dependence of the spin resonance frequency, w_k (normalized to the value $w_d = 7.3 \cdot 10^{-4}$ corresponding to complete beam depolarization) on the proton energy for each of these cases is shown in Fig.4.3. The “dangerous” resonances marked with black dots occure when the values of lg(w_k / w_d) approch zero or -1. As one can see, there are four resonanses in the first case and two resonanses in the second and therd cases.

To preserve polarization, we consider the siberian snake with solenoid magnetic field as an inserted device. The snake containing transverse magnetic field will cause very big closed orbit distortions especially at low energies. The maximum magnetic field integral of the snake depends on the particle momentum and approximately equal to 21 T·m at the Lorenz factor γ=6. It is not necessary to use a full snake to suppress the influence of spin resonances. One can use a partial snake with small longitudinal magnetic field integral.

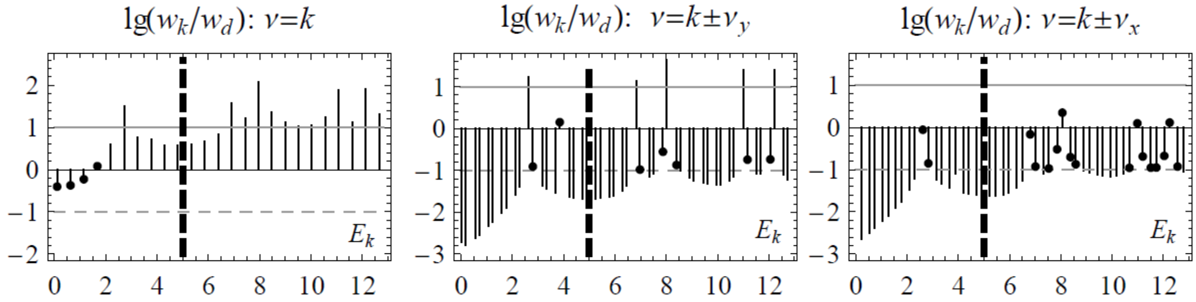

***Fig.4.3**: values of lg(w_k / w_d), caracterizing proton spin resonances in the Nuclotron, vs. the proton energy in GeV,calculated for*: $\nu = k$, $\nu = k \pm \nu_y$, $\nu = k \pm \nu_x$.

If the longitudinal magnetic field is introduced in the synchrotron straight section, the dependence of spin frequency ν on particle energy and spin angle φ_z in the solenoid is defined by a relation: $\cos(\pi\nu) = \cos(\pi\gamma G)\cos\frac{\varphi_z}{2}$. Thus, even with a small longitudinal magnetic field, $\varphi_z/2\pi > |w_k|$, one can completely “exclude” the set of integer resonances, whereas suppressing of the intrinsic resonances is occurred if $\varphi_z/2\pi > |w_k|$. The maximum longitudinal magnetic field integral at $\gamma = 6$ is reached a value of 8.5 T·m, i.e. about twice as less than in the case of the full snake, $(\varphi_z = \pi)$.

The proton spin dynamics along the Nuclotron ring is shown in Fig. 4.4 [9] assuming the snake (full or partial) is placed in the second (after injection) straight section.

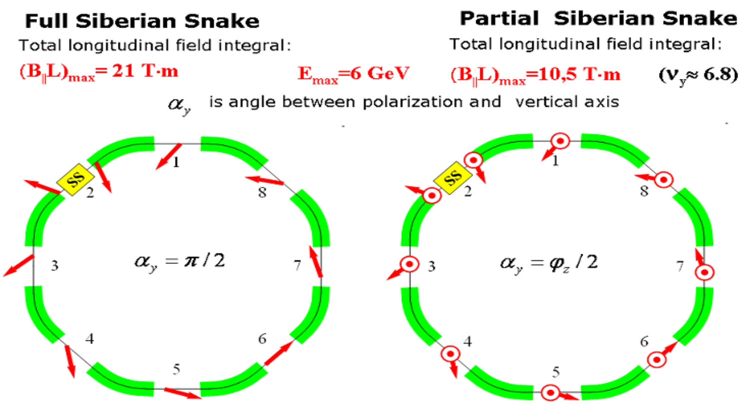

***Fig.4.4:** proton spin dynamics in the Nuclotron ring in the case of a full or partial snake.*

The snake structure – two solenoids and two pair of quadrupoles (G_1,G_2) – and parameters of the insertion are shown in Fig. 4.5.

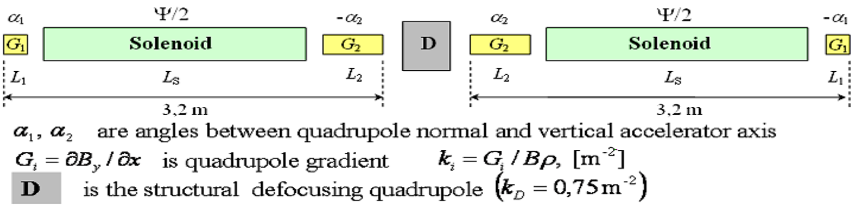

L_S, m	L_1, m	L_2, m	δL, m	α_1	α_2
2,2	0,2	0,5	0,15	50°	50°

Ψ	E_k, GeV	$B_{\|\|}$, T	k_1, m^{-2}	k_2, m^{-2}	G_1, T/m	G_2, T/m	G_D, T/m
$\pi/2$	5/**13**	2,4/**5,6**	0,36	0,75	6,7/**16**	14/**33**	14/**33**
π	**5**/13	**4,8**/11	0,63	1,13	**12**/28	**21**/50	**14**/33

Fig.4.5: *snake structure and parameters of insertion.*

It has been suggested [8] to design universal snakes suitable for any strong focusing magnetic structure of synchrotron or collider, for example to use snakes consisting of solenoids only. In this case the betatron tunes coupling caused by the snake solenoid fringe fields can be compensated by fine tuning of the betatron frequencies. The corresponding case for Nuclotron is shown in Fig.4.6.

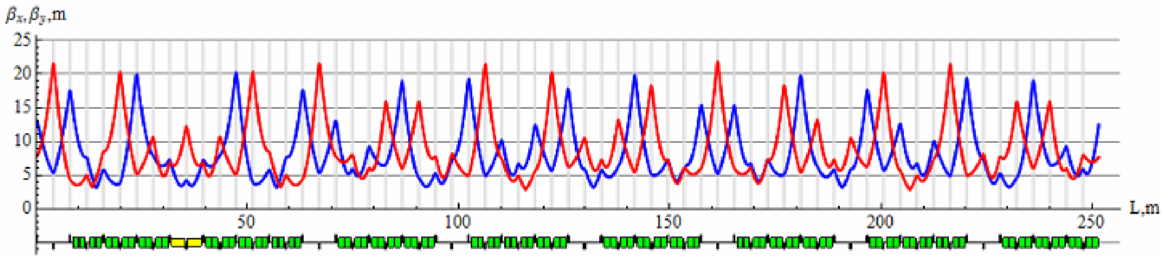

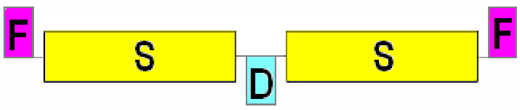

B_{max}, T	K_f, m^{-2}	K_d, m^{-2}	ν_x	ν_y
3.6	0.746	0.753	6.94	6.86

Fig.4.6: *snake consisting of the solenoids only. The snake magnetic field and betatron tune numbers are shown assuming the solenoid length is of 1.5 m.*

4.4. NICA in the polarized proton and deuteron modes.

The novel scheme of the polarization control at NICA, suitable for protons and deuterons, is based on the idea of manipulating polarized beams in the vicinity of the zero spin tune. This approach is actively developed at JLAB for the 8-shaped ring accelerator project. The zero spin tune is a natural regime for the mentioned case.

To provide zero spin tune regime at the collider of the racetrack symmetry, it is necessary to install two identical siberian snakes (Sol π/2) in the opposite straight sections (Fig.4.7). In this scheme any direction of the polarization is reproduced at any azimuth point after every turn. However, if one fixes the longitudinal (or vertical) polarization at SPD, the polarization vector at MPD will be rotated by some angle with respect to the direction of the particle velocity vector. This angle depends on the beam energy. If the direction of the polarization is fixed at MPD, some arbitrary polarization angle will occur at SPD. The control insertions can correct this angle. Solenoid magnetic field integral in a single (Sol π/2)-rotator at maximum energy is about 25 T·m and 80 T·m for protons and deuterons, respectively.

So, feasible schemes of manipulations with polarized protons and deuterons are suggested [10]. The final scheme will be approved at the later stages of the project.

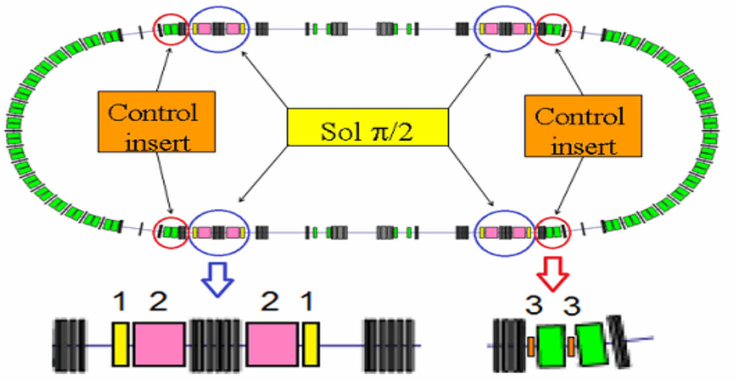

	Type of solenoid	B_{max}	L, m	BL, T·m
1	Pulse	±4	1.25	-5÷5
2	Stationary	9	4	0÷36
3	Weak pulse	±0.5	0.5	-0.25÷0.25

Fig. 4.7: *position of the polarization control elements in the NICA structure.*

4.4.1. NICA luminosity.

The NICA luminosity in the polarized proton mode is estimated for the proton kinetic energy region from 1 to 12.7 GeV [11]. The last value corresponds to the total collision energy $\sqrt{s}$ = 27 GeV and equivalent to the fixed target beam kinetic energy E_{kin_equi} = 388 GeV, Fig. 4.8.

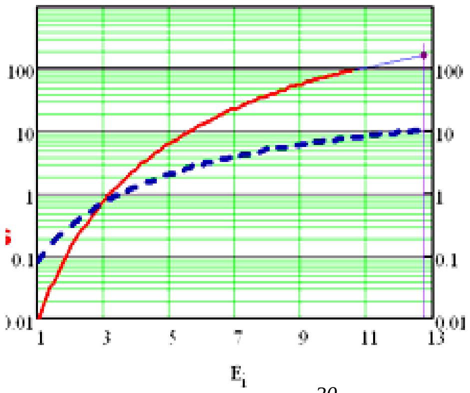

Fig. 4.8: *NICA pp luminosity in units 10^{30} (left scale, solid line) and number of particle per bunch in units 10^{11}(right scale, dotted line).*

The luminosity and total number of the stored particles has been calculated taking into account the beam space charge limits and other parameters listed below.

Parameters of NICA:

circumference - 503 m,
number of collision points (IP) - 2,
beta function β_{min} in the IP - 0.35 m,
number of protons per bunch - $\sim 1\cdot 10^{12}$,
number of bunches - 22,
RMS bunch length - 0.5 m,
incoherent tune shift, $\Delta_{Lasslett}$ - 0.027,
beam-beam parameter, ξ - 0.067,
beam emittance ε_{nrm} (normalized)
at 12.5 GeV, π mm mrad - 0.15.

The number of particles reaches a value about $2.2\cdot 10^{13}$ in each ring and the peak luminosity

$L_{peack} = 2\cdot10^{32}$ $cm^{-2}s^{-1}$ at 12.7 GeV. One can estimate also an average luminosity. Assuming the cooling time T_{cool} = 1500 s, the luminosity life time T_{Llf} = 20000 s and the machine reliability coefficient k_r = 0.95, the average luminosity will be $L_{aver} = L_{peack}\cdot$ 0.86 or $1.7\cdot10^{32}$ cm^{-2} s^{-1} [12].

4.5. Polarimetry at SPI, Nuclotron and NICA. (to be written)

5. Requirements to the spin physics detector (SPD). (UPDATING)

Requirements for SPD are motivated by physics outlined in Section 2 and, first of all, by a topology of events and particles to be recorded. SPD should work at the highest possible luminosity. So, all the SPD sub detectors should have high rate capabilities and preserve high efficiency during a long time. It is useful to remember that in the energy range of NICA the total cross section of *pp* interactions is almost constant, about 40 mb, (Fig.5.1), and expected event rates at the luminosity about 10^{32} sm^{-2} s^{-1} will be about $4\cdot10^6$ per second.

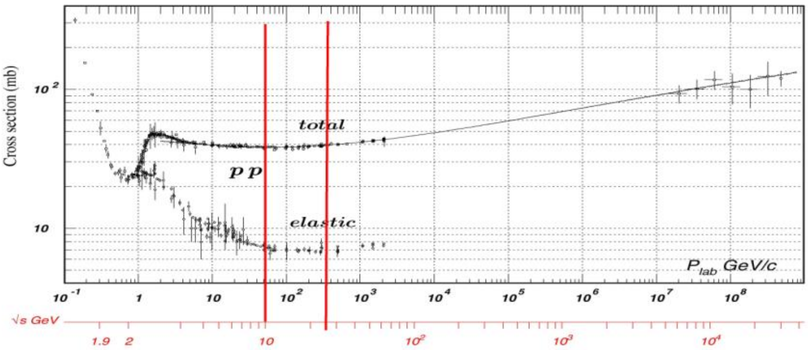

Fig. 5.1: *cross sections of pp interactions versus* $\sqrt{s}$.

The average particle multiplicities estimated with PYTHIA at $\sqrt{s}$ = *24 GeV* are following: charged particles 13.5; neutral particles 22.5; π mesons (+,-,0) 4.6, 3.9, 4.8;K mesons (+,-,0) 0.4,0.3, 0.7.

The typical invariant mass plot for di-lepton production is given in Fig. 5.2. The clean DY events can be detected in region of invariant mass 4 – 9 GeV, below J/Ψ resonances.

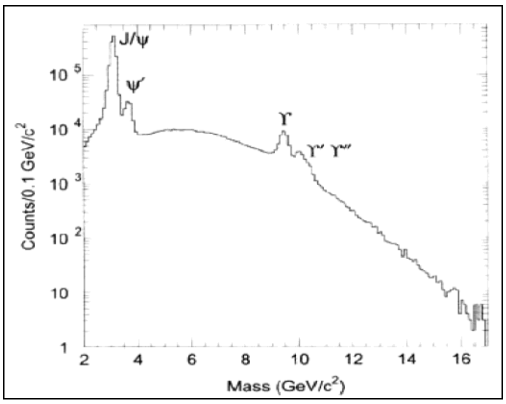

Fig.5.2: *the typical di-lepton invariant mass plot.*

5.1. Event topology.

5.1.1. Topology of DY events.

The Feynman diagram of the *DY* process and configuration of relevant vectors are given in Section 2. For physics purpose lepton pairs must be fully reconstructed using the sub detectors of SPD. To determine a set and characteristics of the SPD sub detectors, the *DY* (μ^-,μ^+) pairs to be recorded were generated by MC method using the PYTHIA 6.4 code. The center of coordinates system was put at the beam intersection point (Z=0, the Z axis is along the beam).

The generated reaction is $pp \rightarrow (\mu^-,\mu^+) + X$, which includes the leading order 2-2 quark level hard scattering sub-processes $q\bar{q} \rightarrow \gamma^* \rightarrow (\mu^-,\mu^+)$. The initial-state radiation (ISR) and final-state radiation (FSR) was switched on. The GRV 94L parameterization [1] of parton distributions was used. The distributions of the di-muon events relevant to this section are shown below.

The di-muon invariant mass distribution is presented in Fig.5.3. The cut $M_{\mu\mu}$ >2 GeV/c^2 was applied for other distributions.

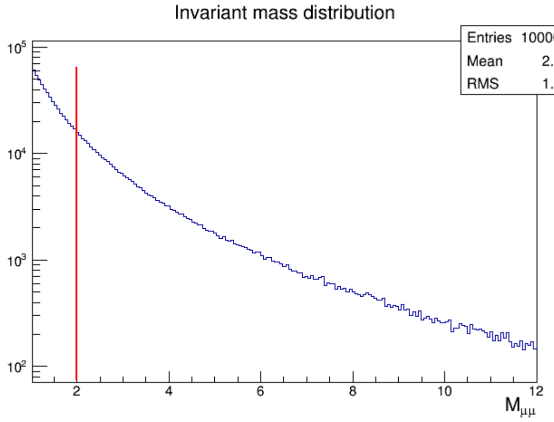

Fig. 5.3*: invariant mass distributions of di-muons.*

Momentum distributions of the single muon from the *DY* pair with the invariant mass $M_{\mu\mu}$ >2 GeV/c^2 for different angular intervals looking from the beam intersection point are shown below (Fig.5.4). The corresponding average momentum is equal to 2.5 GeV /c for all, 1.95 GeV/c for the barrel and 3.5 GeV/c for the end cap muons. So, the momentum of particles to be measured in SPD is in the range from 0 up to 12 GeV. The particle identification system should be able to identify electrons, muons and hadrons in the same momentum range. This is quite simple task for present detectors. For the muon identification the energy-range correlations should be considered.

The distributions of the single muon polar angle measured from Z= 0 and the angle between muons in the Drell-Yan pair are shown in Fig.5.5. Most of the single muons are within the barrel part of the volume. A small part of them passing through the beam pipe will be lost. The minimal and maximal angles between muons are 20º and 180º, respectively. The maximal angles will be also limited by the beam pipe diameter of which should be minimal. These types of angular distributions require almost 4π geometry for the SPD.

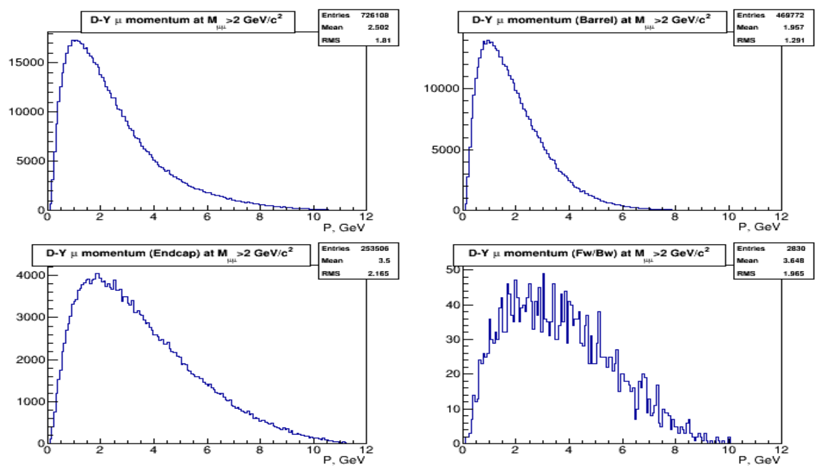

Fig.5.4: *distributions of single muon momentum from the DY events for different angular intervals.* ***Upper:*** *left- all angles; right - $35^0 \div 145^0$.* ***Bottom:*** *left- $3^0 \div 35^0$, right - $0^0 \div 3^0$.*

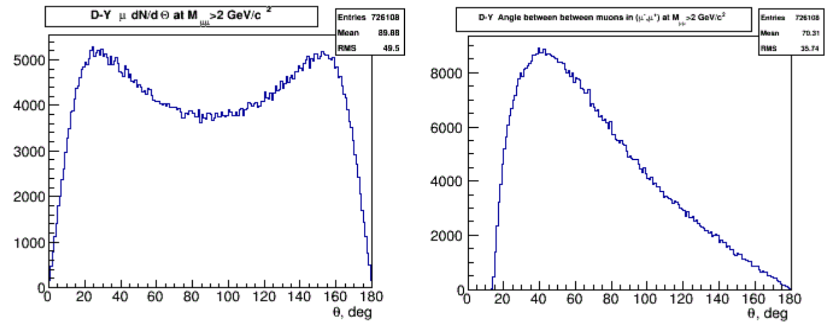

Fig.5.5: *left - single muon polar angle distribution. Right: angle between muons in the pair.*

As it has been checked, generated e^+e^--pairs have almost the same momentum and angular distributions as di-muon pairs.

The distributions of the muon transverse momenta are shown in Fig.5.6.

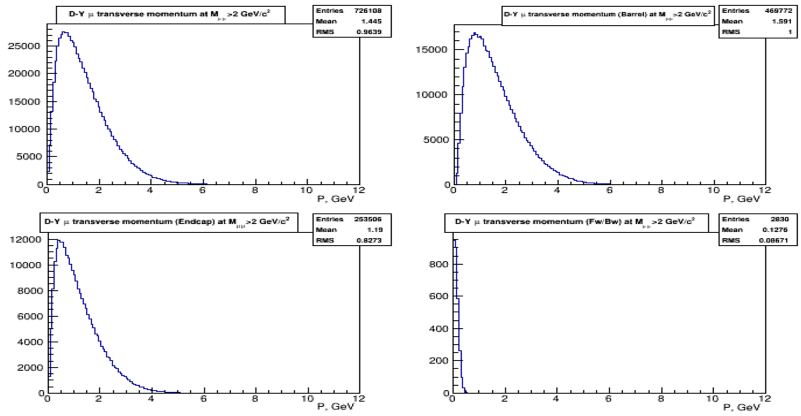

Fig.5.6: *distributions of the muon transverse momenta from the DY events for different angular intervals. Upper: left- all angles; right - $35^0 \div 145^0$. Bottom: left - $3^0 \div 35^0$; right - $0^0 \div 3^0$.*

Taking into account above distributions, for the effective registration of the DY pairs SPD should have :

- almost 4π geometry;
- precision vertex detector;
- precision tracking system ;
- precision momentum measurement;
- muon and électron identification systems.

5.1.2. Topology of J/Ψ events

The *J/Ψ* events produced in *pp* collisions at $\sqrt{s}$ =24 GeV and decayed into the charged lepton pairs have been simulated by MC with the PYTHIA 6.4 generator for the direct production mechanism. This mechanism includes the *J/Ψ* production via the processes of the gluon-gluon, gluon-quark and quark-quark fusions with production of intermediate states and its subsequent decays into the *J/Ψ*. The CTEQ 5L, LO parameterization [2] is used for the PDFs.

The momentum distributions of leptons from *J/Ψ* decays and of the angle between leptons are shown in Fig.5.7.

The correlation between lepton polar angles is shown in Fig.5.8. Most of the lepton pairs (61%) are within the $35^0 \div 145^0$ angular interval; in 35% of pairs one lepton could be found in the $35^0 \div 145^0$ angular interval whiles the other – in the $3^0 \div 35^0$ interval. About 3% of leptons could be registered in the forward and backward $3^0 \div 35^0$ angular intervals. A small part of the pairs will be lost due to beam pipe. These types of angular distributions require almost 4π geometry for SPD.

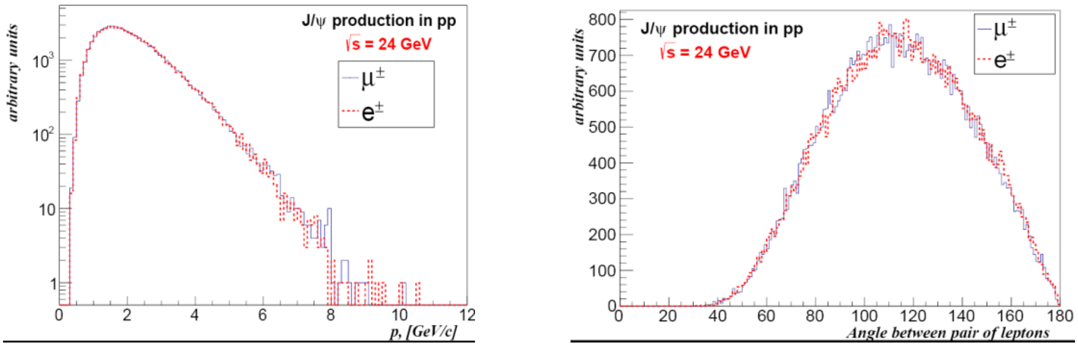

Fig. 5.7: *left - momentum distribution of leptons from J/Ψ decays; right - angle between leptons in the pair.*

The Feynman variable, x_F, and the transverse momentum, p_T, of directly produced *J/Ψ* meson distributions are shown in Fig. 5.9.

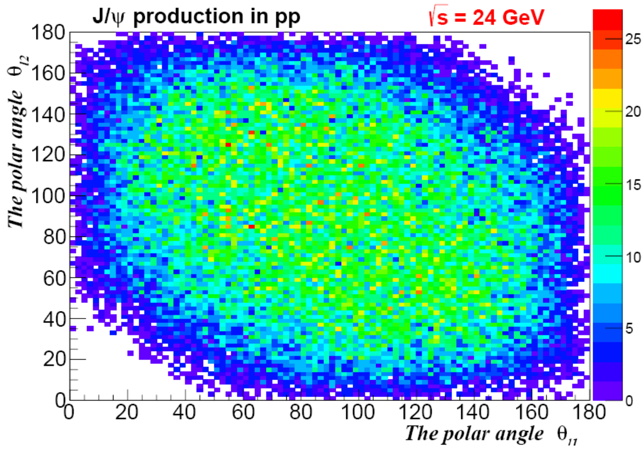

Fig. 5.8: *correlation between lepton polar angles in J/Ψ decays.*

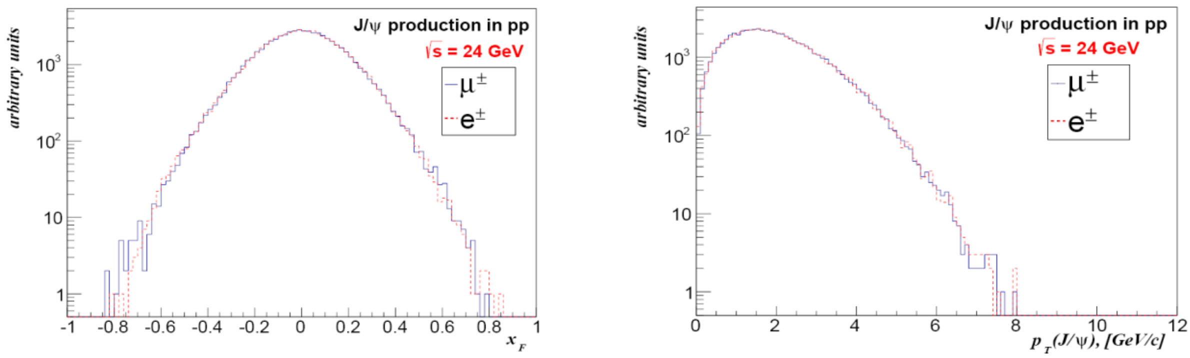

Fig. 5.9: *distributions of directly produced J/Ψ vs. the Feynman variable x_F (left) and vs. the transverse momentum p_T (right).*

5.1.3. Topology of the direct photon production.

A sample of direct photons produced in *pp* collisions at $\sqrt{s}$=24 GeV has been generated by the MC method using the PYTHIA 6.4.2 code. The five hard processes with direct photons in the final state were used: $q+g\to q+\gamma$, $q+qbar\to g+\gamma$, $g+g\to g+\gamma$, $q+qbar\to \gamma+\gamma$ and $g+g\to \gamma+\gamma$. Relative probabilities of the first two processes are 85% and 15%, respectively, while the contribution of all others is less than 0.2%. CTEQ 5L is used for the set of PDFs. No special kinematic cuts are applied. The p_T vs. x_F distribution for direct photons is shown in Fig.5.10.

The photon energy, E_γ, is plotted vs. the photon scattering angle, θ, in Fig. 5.11 (left). The right part of this Figure shows the corresponding plot for minimum bias photons (mainly from π^0 decay). The MC simulations show that for $p_T > 4$ GeV signal-to-background ratio is about 5% that is in good agreement with the data of the UA6 experiment for unpolarized protons at $\sqrt{s}$=24.3 GeV [4].

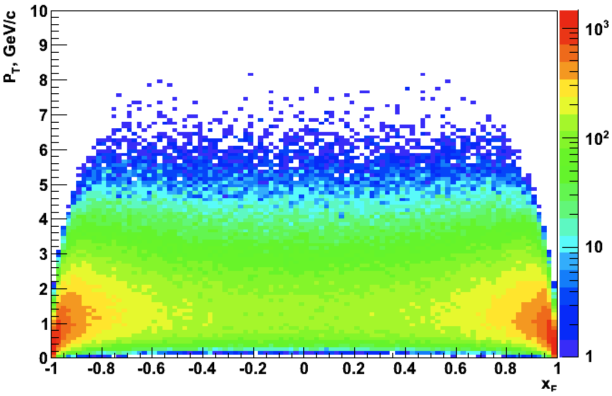

Fig. 5.10: *the plot p_T vs. x_F for direct photons.*

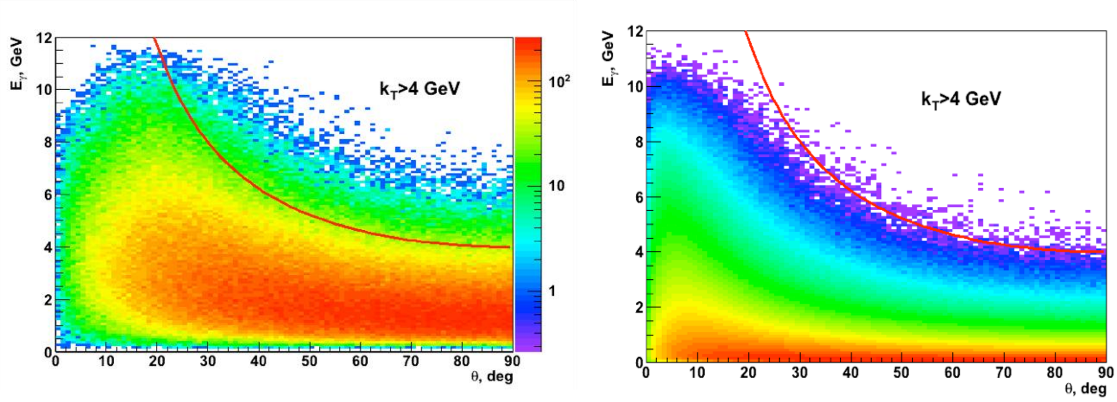

Fig.5.11: distribution of energy E_γ as a function of scattering angle θ: left - direct photons, right - minimum bias photons. Red lines correspond to the cut $p_T > 4$ GeV.

For effective registration and identification of direct photons, SPD should have:

- an electromagnetic calorimeter (ECAL) with a geometry close to 4π and with a granularity optimized to the expected occupancy;
- a tracking system capable to distinguish between clusters from neutral and charged particles in ECAL. It also should be capable to reconstruct the beam interaction point;
- a trigger system based on ECAL. Since for A_N measurements quite energetic photons are needed only, for the main trigger one can require an energy of above 2-3 GeV deposited in any cell of ECAL;
- a DAQ system with a bandwidth up to 100 kHz;
- a luminosity monitor.

5.1.4. Topology of high-p_T reactions. (To be written)

5.2. Possible layout of SPD.

5.2.1. Magnet: toroid vs. solenoid.

Preliminary considerations of the event topologies (Sections 5.1.1 – 5.1.3) require SPD to be equipped with the following sub-detectors covering ~4π angular region around the beam intersection point: vertex detectors, tracking detectors, electromagnetic calorimeters, hadron detectors and muon detectors. Some of them must be in the magnetic field for which there are two options: toroid or solenoid.

A toroid magnet provides a field free region around the interaction point and does not disturb the beam trajectories and polarizations. It can consist of 8 superconducting coils symmetrically placed around the beam axis (see Fig.5.2.1). A support ring upstream (downstream) of the coils hosts the supply lines for electric power and for liquid helium. At the downstream end, a hexagonal plate compensates the magnetic forces to hold the coils in place. The field lines of ideal toroid magnet are always perpendicular to the particles originating from the beam intersection point. Since the field intensity increases inversely proportional to the radial distance: greater bending power is available for particles scattering at smaller angles and having higher momenta. These properties help to design a compact spectrometer that keeps the investment costs for the detector tolerable. The production of such a magnet requires insertion of the coils into the tracking volume occupying a part of the azimuthal acceptance. Preliminary studies show that the use of superconducting coils, made by the *Nb_3Sn-Copper* core surrounded by a winding of aluminium for support and cooling, allows one to reach an azimuthal detector acceptance of about 85%.

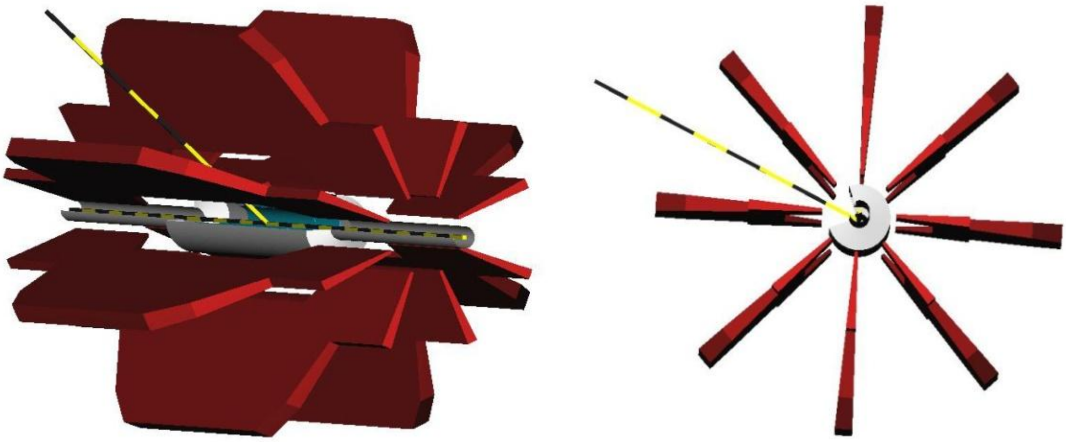

Fig.5.12: *possible view of SPD with the toroid magnet.*

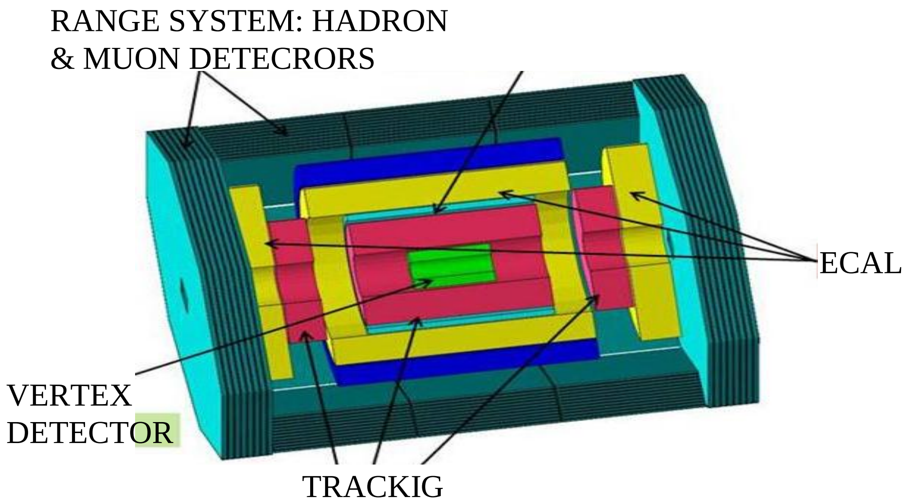

Fig. 5.13: *possible view of SPD with the solenoid magnet.*

Possible SPD layout with the solenoid magnet is shown in Fig.5.13. The magnet part of SPD, usually called “barrel”, contains a vertex detector, tracking detectors and electromagnetic calorimeters (ECAL). Outside of the barrel one needs to have muon and hadron detectors (Range system). The end cup part of SPD could contain a tracking, ECAL, muon and range systems. The solenoid SPD version could have almost 100% azimuthal acceptance, which is important for example for detection of some exclusive reactions. Disadvantage of the solenoid is presence of the magnetic field in the beam pipe region. This field can disturb beam particle trajectories and their polarization

The dimension of the SPD volume is still an open question. It should be optimized basing on compromise between the precisions and costs. The "almost 4πgeometry" requested by DY and direct photons can be realized in the solenoid version of SPD if it has overall length and diameter of about 6 m.

5.2.2. Vertex detector.

The most obvious version of vertex detector is a silicon one. Several layers of double sided silicon strips can provide a precise vertex reconstruction and tracking of the particles before they reach the general SPD tracking system. The design should use a small number of silicon layers to minimize the radiation length of the material. With a pitch of 50-100 μm it is possible to reach a spatial resolution of 20-30 μm. Such a spatial resolution would provide 50-80 μm for precision of the vertex reconstruction. This permits to reject the secondary decay vertexes.

The elements of the SPD vertex detector can be of the same design as for MPD [5].

5.2.3. Tracking.

There are several candidates for a tracking system: multiwire proportional chambers (MWPC), conventional drift chambers (DC) and their modification – thin wall drift tubes (straw chambers). The DCs are the good candidates for tracking detectors in the end cup parts of SPD, while straw chambers are the best for the barrel part.

Two groups have developed the technology of straw chamber production at JINR [6] with two-coordinate reed out. The radial coordinate determination is organized via the electron drift time measurement while the measurement of the coordinate along the wire (z-coordinate) uses the cathode surface of the straw. Both technologies provide a radial coordinate resolution of 150-200 μm per plane. The chambers, assembled in modules consisting of several pairs of tracking planes, can have the radial coordinate resolution of about 50 μm. This can provide the momentum resolution of the order of 10 % over the kinematic range of the NICA. Straw tubes used by Baranov et al. are made of the 30 micron nylon tape and have the coordinate resolution along the anode of about 1mm, while the Bazilev et al. tubes are made of double layers kapton of 25 micron thick (minimum) and have resolution along the anode of about 1 cm.

5.2.4. Electromagnetic calorimeters.

The latest version of the electromagnetic calorimeter (ECAL) module, developed at JINR for the COMPASS-II experiment at CERN, Fig.5.14 [7], can be a good candidate for ECAL in the barrel and end cup parts of SPD. The module utilises new photon detector – Avalanche Multichannel Photon Detector (AMPD). AMPD can work in the strong magnetic field. The modules have rectangular shape but can be produced also in the projection geometry which is better for SPD. The energy resolution of the module is about 10% at 1GeV. The modules have a fast readout and can be used in the SPD trigger system.

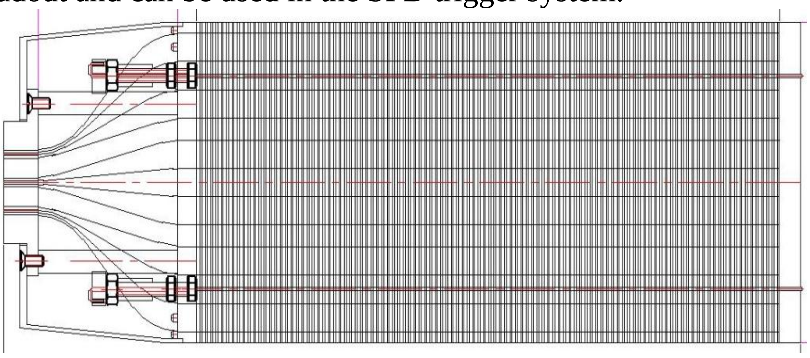

Fig.5.14: *ECAL module structure.*

The module has 109 plates of the scintillator and absorber (Pb) of 12x12 cm in cross section and 0.8 and 1.5 mm thick, respectively. The radiation length and Moliere radius is 1.64 and 3.5 cm, respectively. The light collection is performed with optical fibers dividing the module in nine logical sections (towers).

5.2.5. Hadron (muon) detectors

A system of mini-drift chambers interleaved with layers of iron is called the Range System (RS) developed at JINR for FAIR/PANDA [8] (see Fig.5.15). It can be used in the barrel part of SPD as a hadron and (or) muon detector for the Particle IDentification system (PID). RS can provide clean (> 99%) muon identification for muon energies greater than 1 GeV. The combination of responses from ECAL, RS and momentum reconstruction can be used for the identification of electrons, hadrons and muons in the energy range of the NICA SPD.

The hadron and muon detectors in the end caps part of SPD are to be identified. As candidates for these detectors the COMPASS muon wall [9] can be considered. It consists of two layers of mini-drift chambers with a block of absorber between them.

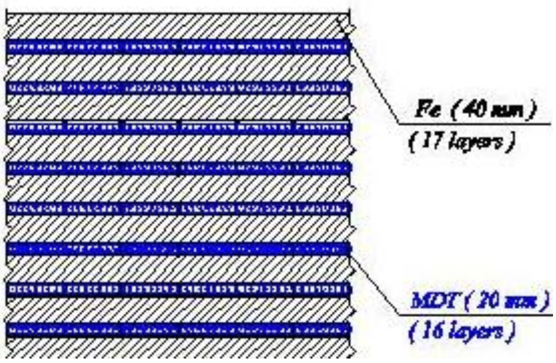

Fig. 5.15: *scheme of the RS. Dimension and thickness are subjects of optimization.*

5.3. Trigger system. (**To be updated**)

The main task of the trigger system is to provide separation of a particular reaction from all reactions occurred in collisions. Each of them will be pre-scaled with:

- two muons in the final state;
- electrons/positron pair in the final state;
- direct photons (π^0, ω, η…);
- various types of hadrons in final states (π+/-, K, p, …);
- other reactions.

Hodoscopes of scintillating counters and resistive plate chambers (RPC, Fig.5.16 [10]) are proposed as detectors for the SPD trigger system. The hodoscopes can be located before and after RS (or mounted in the last layers of RS) and before ECAL. The ECAL modules will also be used in the trigger system. The trigger system should consist of several layers.

5.4. Local polarimeters and luminosity monitors (to be updated)

5.4.1. Local polarimeters

Local polarimeters should provide information on the beam (s) polarization (s) at the beam intersection point. It means they should be incorporated in the SPD sub-detector system. Reactions, which can be used for this purpose, are inclusive production of π^0 and $\pi^{\pm}$ mesons.

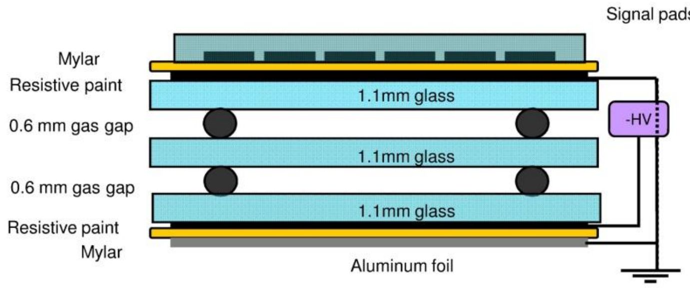

Fig.5.16: scheme of the RPC unit

5.4.2. Local luminosity monitors.

The luminosity monitoring at SPD can be performed with the Zero Degree Calorimeters (ZDC) similar to those used at RHIC [10]. The design of ZDCs will be proposed after finalizing the design of SPD.

5.5. Engineering infrastructure (to be updated)

5.5.1. Experimental area.

The plan view of the experimental area for SPD, extracted from the official NICA construction documents (see draw. 318Б-063К-АР-АР, sheet 3), is shown in Fig.5.16.

SPD and technological equipment necessary for assembly and commissioning will be accommodated in a pavilion to be constructed around the second intersection point of the Collider. The detector itself in the working position will be located in the room 128/1. Assembling and maintenance of the detector can be performed in the room 128/2. This room is a garage position for SPD with all systems between the working sessions of the complex.

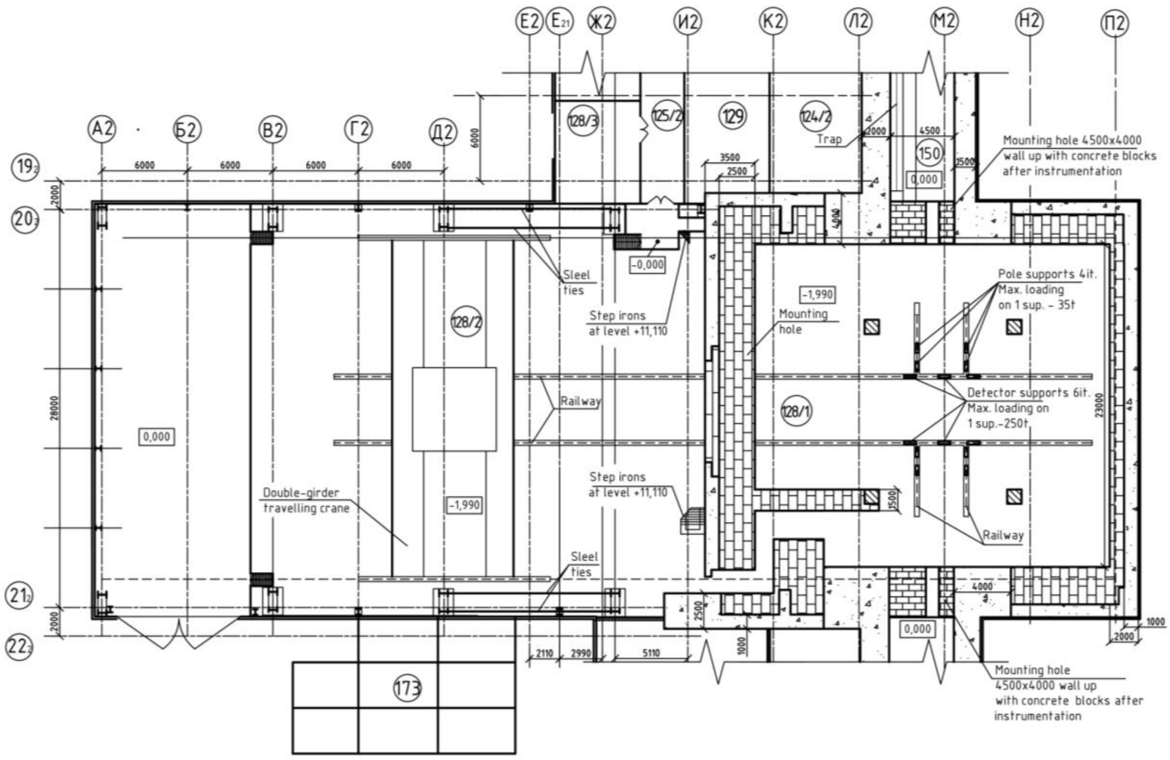

Fig.5.16: plan view of the SPD experimental area.

Dimension of the room (along/across the beams) is: for 128/1 – 22.5 m x 25 m= 562.5 m^2, for

128/2 – 24 m x 42 m = 1008 m^2. Both rooms have a height 19.85 m from the floor level to the roof. The floor is reinforced to keep the uniformly distributed weight 2t/m^2 in the room 128/1 and 16t/m^2 in 128/2. The whole area (128/1 and 128/2) is located in a hollow, depth 3.49 m below the median plane of the Collider (1.99 m below clean floor level of the Collider). SPD, assembled on a rolling cart platform in the room 128/2, will be transported to 128/1 by rails. The total weight of assembled SPD should be less than 600 tons.

The assembly room 128/2 is equipped with a bridge crane of 50 tons lifting capacity. Crane provides the movement of the SPD components from the unloading space to the assembly space. The height from the floor to the bottom of the crane hook is 15 meters. The crane service zone is 22 m long in transverse direction. The crane has additional hook with lifting capacity of 10 tons.

5.6. DAQ (to be written)
5.7. SPD reconstruction software (to be written)
5.8. Monte Carlo simulation software (to be written)
5.9. Slow control **(to be written)**

6. Proposed measurements with SPD. (UPDATING)

We propose to perform measurements of asymmetries of the DY pairs production in collisions of polarized protons and deuterons (Eqs.2.1.0) which provide an access to all collinear and TMD PDFs of quarks and anti-quarks in nucleons. The measurements of asymmetries in production of J/Ψ and direct photons will be performed simultaneously with DY using dedicated triggers. The set of these measurements will supply complete information for tests of the quark-parton model of nucleons at the twist-two level with minimal systematic errors.

6.1. Estimations of DY and J/Ψ production rates.

6.1.1. Estimations of the DY production rates and precisions of asymmetry measurements.

Estimation of the DY pair's production rate at SPD was performed using the expression [1] for the differential and total cross sections of the *pp* interactions:

$$\frac{d^2\sigma}{dQ^2dx_1} = \frac{1}{sx_1}\frac{4\pi\alpha^2}{9Q^2}\sum_{f,\bar{f}} e_f^2[f(x_1,Q^2)\bar{f}(x_2,Q^2)]_{x_2=Q^2/sx_1}$$

$$\sigma_{tot} = \int_{Q^2_{min}}^{Q^2_{max}} dQ^2 \int_{x_{min}}^{1} dx_1 \frac{d^2\sigma}{dQ^2dx_1},$$

where Q is the invariant mass of lepton pair, $M_{l\text{-}l+}$, x_1 (x_2)≡ x_a (x_b) is the Bjorken variable of colliding hadron, s is the *pp* center of mass energy squared. The Table 1 shows values of the cross-sections and expected statistics for DY events per year (7000 hours of NICA and 100% acceptance of SPD) at two energies.

Table 1: estimation of the cross-section and number of DY events for SPD-NICA per year.

Lower cut on M_{l+l-}, *GeV*	2.0	3.0	3.5	4.0
$\sqrt{s}=24$ *GeV* ($L \approx 1.0\ 10^{32}$ $cm^{-2}\ s^{-1}$)				
σ_{DY} total, *nb*	1.15	0.20	0.12	0.06
events per year, 10^3	1800	313	179	92
$\sqrt{s}=26$ *GeV* ($L \approx 1.2\ 10^{32}$ $cm^{-2}\ s^{-1}$)				
σ_{DY} total, *nb*	1.30	0.24	0.14	0.07
events per year, 10^3	2490	460	269	142

The dependence of the total cross section and of number of DY events per year versus the cut on the minimal $M_{l^-l^+}$ is shown in Fig.6.1.

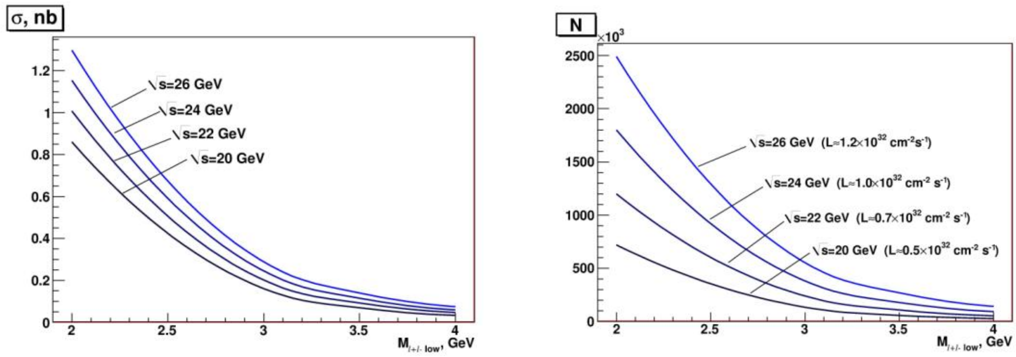

***Fig.6.1**: cross section (left) and number of DY events (right) versus the minimal invariant mass of lepton pair for various proton beam energies.*

To estimate the precision of measurements, the set of original software packages for MC simulations, including generators for Sivers, Boer-Mulders and transversity PDFs were developed [2]. With these packages we have generated a sample of 100K DY events in the region $Q^2 > 11$ GeV^2 for comparison with expected asymmetries.

Let us first estimate the q_T- weighted integrated asymmetry (Sivers) $A_{UT}^{w\left[\sin(\phi-\phi_S)\frac{q_T}{M_N}\right]}\Big|_{pp^\uparrow\to l^+l^-X}$ given by Eq. (2.1.12). For this purpose we have used three different fits for the Sivers function: Fit I: $xf_{1uT}^{\perp(1)} = -xf_{1dT}^{\perp(1)} = 0.4x(1-x)^5$ and Fit II: $xf_{1uT}^{\perp(1)} = -xf_{1dT}^{\perp(1)} = 0.1x^{0.3}(1-x)^5$ of Ref.[3] and Fit III: $xf_{1uT}^{\perp(1)} = -xf_{1dT}^{\perp(1)} = (0.17...0.18)x^{0.66}(1-x)^5$ of Ref. [4]. For the first moment of the Sivers PDF entering Eq. (2.1.12) we used the model (with the positive sign) proposed in Ref. [4]:

$$\frac{\bar{f}_{1qT}^{\perp(1)}}{f_{1qT}^{\perp(1)}} = \frac{\bar{f}_{1u}(x)+\bar{f}_{1d}(x)}{f_{1u}(x)+f_{1d}(x)}. \qquad (2.1.25)$$

The estimated asymmetry as a function of $x_p - x_{p\uparrow}$ is shown in Fig.6.2.

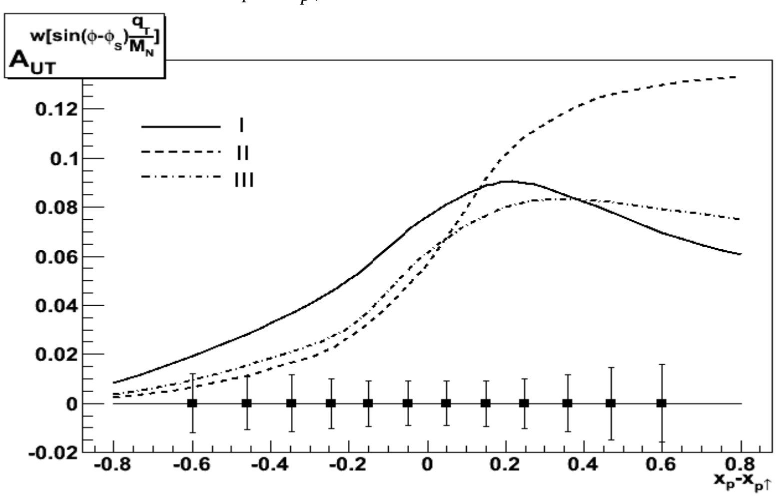

***Fig.6.2:** estimated Sivers asymmetry $A_{UT}^{w\left[\sin(\phi-\phi_S)\frac{q_T}{M_N}\right]}$ at $\sqrt{s}$ =26 GeV with Q^2 = 15 GeV^2. Numbers I, II, III denote corresponding fits. Points show the expected errors obtained with 100K of events.*

As one can see from this Figure, the expected integrated Sivers asymmetries depend on the Sivers PDF parameterization and vary in the whole region of $x_p - x_{p\uparrow}$ from about 1 to 12%. Statistics of 100K is marginally enough to distinguish the fits.

Let us now estimate the asymmetry $A_{UT}^{w\left[\sin(\phi+\phi_S)\frac{q_T}{M_N}\right]}\Big|_{pp\uparrow}$ given by Eq. (2.1.13). Since the Boer-Mulders PDF and its first moment are still poorly known, we have used the Boer's model (Eq. (50) in Ref.[5]) which provides the good fit for the NA10 [6] and E615 [7] data on the anomalously large cos*(2φ)* dependence of DY cross sections. This model gives for the first moment (2.1.15) entering Eq. (2.1.13) the value $h_{1q}^{\perp(1)}(x) = 0.163 f_1(x)$. For the first moment of the Boer-Mulders sea part PDF, we assumed a relation

$$\frac{\bar{h}_{1qT}^{\perp(1)}(x)}{h_{1T}^{\perp(1)q}(x)} = \frac{\bar{f}_{1q}(x)}{f_{1q}(x)}.$$

The transversity PDF h_1 was extracted recently from the combined data of HERMES, COMPASS and BELLE collaborations. However, because of the rather big errors in the data, in a course of extraction a number of approximations were used. Particularly the zero sea transversity PDF was assumed. But, in the case of *pp* collisions, the sea PDFs play the important role. That is why two versions of the evolution model for the transversity are considered here. In the first version of the model the transversity for quarks and anti-quarks

$$h_{1q}(x,Q_0^2) = \frac{1}{2}\left[q(x,Q_0^2) + \Delta q(x,Q_0^2)\right],\;\; \bar{h}_{1q}(x,Q_0^2) = \frac{1}{2}\left[\bar{q}(x,Q_0^2) + \Delta\bar{q}(x,Q_0^2)\right]$$

are assumed to be equal to the helicity PDF Δq ($h_{1q} = \Delta q,\ \bar{h}_{1q} = \Delta\bar{q}$) at the low initial $Q_0^2 = 0.23\ GeV^2$, and then they are evolved with DGLAP equations. In the second model [8, 9] the transversity PDFs are assumed to be equal to $h_{1q} = (\Delta q + q)/2$ *and* $\bar{h}_{1q} = (\Delta\bar{q} + \bar{q})/2$ at the same initial scale, and then h_{1q} and $\bar{h}_{1q}$ are again evolved with DGLAP. This model we consider as more realistic one. The results of estimations for the NICA energy are presented in Fig. 6.3. As one can see, in the both models the Boer-Mulders asymmetry is rather large at negative values of $x_p - x_{p\uparrow}$. At the positive values of $x_p - x_{p\uparrow}$ the asymmetry is model dependent. With statistics of about 100K DY events one can distinguish the models.

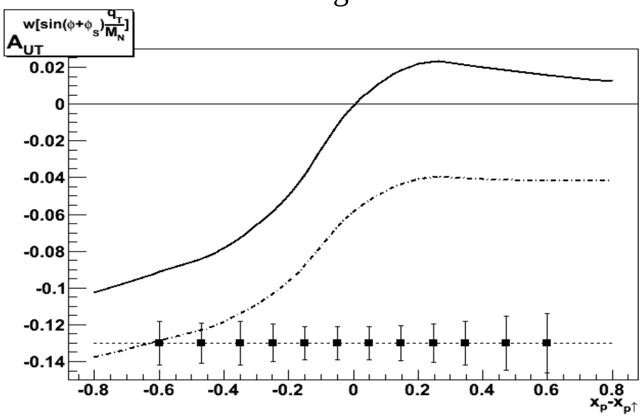

Fig.6.3: *estimations of Boer-Mulders asymmetry* $A_{UT}^{w\left[\sin(\phi+\phi_S)\frac{q_T}{M_N}\right]}$ *at* $\sqrt{s}$ *=26 GeV with* Q^2 *= 15* GeV^2*. The solid and dotted curves correspond to the first and second versions of the evolution model, respectively. Points show the expected errors obtained with 100K of events.*

6.1.2. Estimations of the J/ψ production rates and precisions of asymmetry measurements.

Statistics of the J/ψ and DY events (with cut on M_{l-l+} = 4 GeV) expected to be recorded in one year of NICA operation (7000 hours) with 100% efficiency of SPD is given in Table 2 below.

Table 2: comparison of the J/ψ and DY statistics

√s , GeV	*24*	*26*	*√s , GeV*	*24*	*26*
$\sigma_{J/\psi}$, B_{e+e-} , nb	*12*	*16*	*σ_{DY} , nb*	*0.06*	*0.07*
Events per year	***$18\cdot10^6$***	***$23\cdot10^6$***	*Events per year*	***$92\cdot10^3$***	***$142\cdot10^3$***

Accessible ranges of the Bjorken variables for asymmetry measurements with the DY or J/ψ events are shown in Fig.6.4.

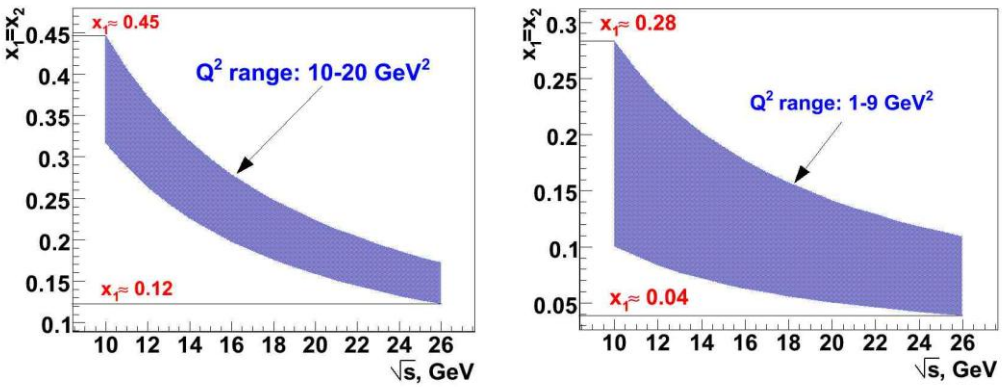

***Fig.6.4:** ranges of the Bjorken variable vs. √s for DY (left) and J/Ψ (right) measurements.*

6.2. Estimations of direct photon production rates.

Estimation of the direct photon production rates based on PYTHIA6 Monte-Carlo simulation is presented in Table 3 for two values of colliding proton energies. Event rates are given for all and for leading processes of direct photon production considered in PYTHIA (see Table in Appendix 1) assuming that 1 year is equivalent to 7000 hours of operation at maximal luminosity. The last column gives the rates with the cut on the transverse momentum of photons suggested in Section 5.1.3.

To estimate statistical accuracy of A_N and A_{LL} measurement at NICA suggested in Section 2.3 one can assume that the beam polarizations (both transversal and longitudinal) are equal to P=±0.8 and overall detector efficiency (acceptance, efficiency of event reconstruction and selection criteria) is about 50%. Under such assumption, after 1 year of data taking the A_N and A_{LL} could be measured with statistical accuracy ~0.11% and ~0.18%, respectively, in each of 18 x_F bins (-0.9< x_F < +0.9). Large statistics of events provide opportunities to measure the asymmetries as a function of x_F and p_T.

To minimize systematic uncertainties, precision of luminosity and beam polarization should be under control, as well as accuracy of π^0 , η and other background rejection.

Table 3: Estimated rates of the direct photon production.

$\sqrt{s}$=24 GeV $L = 1.0\times10^{32},\ cm^{-1}s^{-1}$	σ_{tot}, nbarn	$\sigma_{P_T>4\ GeV/c}$, nbarn	Events/year, 10^6	Events/year, 10^6 $(P_T > 4\ GeV/c)$
All processes	1290	42	3260	105
$qg \to q\gamma$	1080	33	2730	84
$q\bar{q} \to g\gamma$	210	9	530	21
$\sqrt{s}$=26 GeV $L = 1.2\times10^{32},\ cm^{-1}s^{-1}$	σ_{tot}, nbarn	$\sigma_{P_T>4\ GeV/c}$, nbarn	Events/year, 10^6	Events/year, 10^6 $(P_T > 4\ GeV/c)$
All processes	1440	48	4340	144
$qg \to q\gamma$	1220	38	3680	116
$q\bar{q} \to g\gamma$	240	10	660	28

6.3 – 6.5. **TO BE WRITTEN**

7. Time lines of experiments.

The participants of the LoI are planning to submit the document for discussions at the JINR and outside during the year 2014. If it will be approved at JINR by the end of 2014, the corresponding Proposal including the time lines of experiments could be prepared by the end of 2015.

8. References.

8.1. References to Section 1.

[1] http://nica.jinr.ru/files/SPIN_program/NICA-SPD2013/index.html
http://nica.jinr.ru/files/SPIN_program/SPIN-Praha-2013/index.html
http://theor.jinr.ru/~spin/2013/

[2] I.A. Savin and A.P. Nagaytsev. Physics of the elementary particles and atomic nuclei, 2004, t. 35, iss. 1 and references therein.

[3] O. Shevchenko, QCD

[4] C. Marchand, in Proceedings of the XX International Workshop on Deep-Inelastic Scattering and Related Subjects, Bonn, Germany, 26-30 March 2012.

[5] B. Parsamyan, Talk @ DIS 2013.

8.2. References to Section 2.

[1] J.C. Collins and D.E. Soper, Phys. Rev. D 16, 2219 (1977).

[2] J.C. Collins, D.E. Soper, and G. Sterman, Nucl. Phys. B250, 199 (1985).

[3] X. Ji, J.P. Ma, and F. Yuan, Phys. Rev. D 71, 034005 (2005) [arXiv:hep-ph/0404183].

[4] J.C. Collins and A. Metz, Phys. Rev. Lett. 93, 252001 (2004) [arXiv:hep-ph/0408249].

[5] S. Arnold, A. Metz and M. Schlegel, Phys.Rev. D79 (2009) 034005 [arXiv:hep-ph/0809.2262]

[6] L.P. Gamberg, D.S. Hwang, A. Metz, and M. Schlegel, Phys. Lett. B 639, 508 (2006) [arXiv:hep-ph/0604022].

[7] A. Bacchetta, D. Boer, M. Diehl, and P. J. Mulders, JHEP 0808, 023 (2008) [arXiv:0803.0227 [hep-ph]].

[8] M. Anselmino, M. Boglione, U. D'Alesio, S. Melis, F. Murgia, A. Prokudin, arXiv:1304.7691 [hep-ph].

[9] Daniel Boer, Leonard Gamberg, Bernhard Musch, Alexei Prokudin, JHEP 1110 (2011) 021 [arXiv:1107.5294].

[10] P.J. Mulders and R.D. Tangerman, Nucl. Phys. B461, 197 (1996) [Erratum-ibid. B484, 538 (1997)] [arXiv:hep-ph/9510301].

[11] A. Bacchetta, M. Diehl, K. Goeke, A. Metz, P. Mulders and M. Schlegel, JHEP 0702, 093 (2007) [arXiv:hep-ph/0611265].

[12] S.J. Brodsky, D.S. Hwang, and I. Schmidt, Phys. Lett. B 530, 99 (2002) [arXiv:hep-ph/0201296].

[13] J.C. Collins, Phys. Lett. B 536, 43 (2002) [arXiv:hep-ph/0204004].

[14] S.J. Brodsky, D.S. Hwang, and I. Schmidt, Nucl. Phys. B642, 344 (2002) [arXiv:hep-ph/0206259].

[15] A. Sissakian, O. Shevchenko, A. Nagaytsev, and O. Ivanov, arXiv:0807.2480 [hep-ph].

[16] A. Sissakian, O. Shevchenko, A. Nagaytsev and O. Ivanov, Phys. Rev. D 72, 054027 (2005) [arXiv:hep-ph/0505214].

[17] A. Sissakian, O. Shevchenko, A. Nagaytsev, O. Denisov, and O. Ivanov, Eur. Phys. J. C 46, 147 (2006) [arXiv:hep-ph/0512095].

[18] J.J. Aubert et al., [E598 Collaboration], Phys. Rev. Lett. 33(1974)1404.

[19] J.E. Augustin et al., [SLAC-SP-017 Collaboration], Phys. Rev. Lett. 33(1974)1406.

[20] S.J. Brodsky and J.-P. Lansberg, Phys. Rev. D 81(2010) 051502 [arXiv:0908.0754 [hep-ph]].

[21] T.Sjostrand, S.Mrenna and P.Z.Skands, ``PYTHIA 6.4 Physics and Manual", JHEP 0605 (2006) 026 [hep-ph/0603175].

[22] N. Anselmino, V. Barone, A. Drago, N. Nikolaev, Phys. Lett. B594 (2004) 97

[23] E. Leader and E. Predazzi, ``Introduction to Gauge Theories and the ``New Physics`, Cambridge Univ. Press. 1982.

[24] V. Barone, Z. Lu, B. Ma, Eur. Phys. J. C49 (2007) 967.

[25] I. Shmidt, J. Soffer and J.J. Yang, Phys. Lett. B 612 (2005) 258-262.

[26] J. Qui and G. Sterman, Phys. Rev. Lett. 67 (1991) 2264; Nucl. Phys. B 378 (1992) 52.

[27] J. Xiandong, Phys. Lett. B 289 (1992) 137.

[28] N. Hammon et al., Phys. G: Nucl. Part. Phys. 24 (1998) 991-1001.
[29] L. Gamberg and Z. Kang, Phys. Lett. B 718 (2012) 181.
[30] D. L. Adams et al., Phys. Lett. B 345 (1995) 569-575.
[31] S. Campbell: "Prompt photon measurements with PHENIX's MPC-EX detector", talk at Nuclear Dynamics 2013, https://www.phenix.bnl.gov/phenix/WWW/talk/archive/2013/ndww13/t2103.pdf
[32] Len K. Eun, http://meetings.aps.org/link/BAPS.2011.DNP.HC.3.
[33] Cheng HY, Lai SN. Phys. Rev. D 41:91 (1990) 91-102.
[34] G. Bunce et al., Ann.Rev.Nucl.Part.Sci.50:525-575, (2000).
[35] V. Baryshevsky, World Scientific, Singapore (2012) 1-640. ISBN-13: 9789814324830.
[36] H. Seyfarth et al., Phys. Rev. Lett. 104 (2010) 222501.
[37] L. S. Azhgirei et al., Physics of Particles and Nuclei Letters 7(2010) 27.
[38] NA51 Collaboration, M.C. Abreu et al, Phys. Lett. B438 (1998) 35-40.
[39] E866: Proposal for Drell-Yan Measurements of Nucleon and Nuclear Structure with the FNAL Main Injector, April 9. 1999
[40] COMPASS-II Proposal, CERN-SPSC-2010-014, SPSC-P-340, May 2010.
[41] E906: L.D. Isenhower at al., Drell-Ayn Measurements of Nucleon and NUclear Structure wih FNAL Main Injector, Funding Proposal submitted to US DOE, May 2012, http://www.phy.anl.gov/mep/SeaQuest/.
[42] PANDA Collaboration, Technical Design Report on the PANDA Muon System, May 2012 .
[43] RHIC: Les Bland et al., Transverse Spin Drell-Yan Physics at RHIC, May 2007;
M.G. Perdekamp, Future Drell-Yan Collider Experiments, Talk presented at international workshop 'Studying the hadron strucure in Drell-Yan reactions", CERN April 2010;
Elke-Caroline Aschenauer et al., The RHIC SPIN Program, Achievements and Future Opportunities, 2012, http://www.bnl.gov/npp/docs/RHIC-Spin-WriteUp-121105.pdf;
G.Bunce et al., Plans for RHIC Spin Physics Program, June 2008, http://spin.riken.bnl.gov/rsc/report/spinplan_2008/spinplan08.pdf

8.4. References for Section 4.

[1]. V.D.Kekelidze, A.D.Kovalenko, R.Lednicky, V.A.Matveev, I.N.Meshkov, A.S.Sorin, G.V. Trubnikov. Status of NICA project at JINR. PoS(Baldin ISHEPP XXI) 085, pp 1-9, SISSA. It.
[2]. A.D.Kovalenko et al. The NICA Facility in Polarized Proton Operation Mode, IPAC'2011 http://accelconf.web.cern.ch/AccelConf/IPAC2011/papers/tupz004.pdf
[3]. V.Fimushkin, A.S.Belov, A.D.Kovalenko et al. EPJ, Special Topics, 162, pp. 275-280, (2008), Springer/
[4]. V.Fimushkin et al. Physics of Part.&Nucl., 2014, Vol. 45, No.1, pp. 297-300,Springer 2014.
[5]. A.Butenko et al. Development of the NICA Injection Facility
[6]. N.G.Anishchenko et al. Journ. de Phys. Colloquia C2, Vol.46, C2-703, (1985)
[7]. S.Vokal, A.D.Kovalenko, A.M.Kondratenko et al. Physics of Part.&Nucl., 2009, Vol. 6, No.1, pp. 48-58, Springer 2009.
[8] Yu.N.Filatov, A.D.Kovalenko, A.V.Butenko et al. Physics of Part.&Nucl., 2014, Vol. 45, No.1, pp. 262-264,Springer 2014.
[9]. M.A.Kondratenko et al. Orbital Parameters of Proton Beam in Nuclotron with Solenoid Siberian Snake. XV Workshop DSPIN'2013, Dubna, October 8-12, 2013 (to be published).
[10]. Yu.N.Filatov, A.M.Kondratenko, A.D. Kovalenko et al. Proton and Deuteron Polarization Control in NICA Collider Using Small Soplenoids. XV Workshop DSPIN'2013, Dubna, October 8-12, 2013 (to be published).
[11]. I.N.Meshkov. privat communication
[12]. A.D.Kovalenko. Polarized Deuterons and Protons at NICA: Status of the Design Concept. XV Workshop DSPIN'2013, Dubna, October 8-12, 2013 (to be published).

8.5. References for Section 5.

[1] GRV 94
[2] STEQ 5L
[3]
[4] UA6
[5.] Yu. Murin and M. Merkin, talks at the International Workshop "ADVANCED STUDIES INSTITUTE SYMMETRIES AND SPIN", Prague, July 2013.
[6] S.N. Bazylev et al., JINR preprint P13-2010-69, NIM A 632 (2011) 75; K.I. Davkov et al., JINR Preprint P13-2012-93, PTE, 2013,N.4,1.
V.A. Baranov (Dubna, JINR), B.A. Chekhovskiy (Minsk, NCPHEP), N.P. Kravchuk, A.S. Korenchenko, N.A. Kuchinskiy, N.V. Khomutov, S.A. Movchan, V.S. Smirnov (Dubna, JINR), F.E. Zyazyulya (Minsk, NCPHEP), **Instrum.Exp.Tech. 55 (2012) 26-28, arXiv:1105.2258 [physics.ins-det] | PDF**

[7] N. Anfimof et al., COMPASS Note 2011-2; N. Anfimov, talk at the International Workshop “ADVANCED STUDIES INSTITUTE SYMMETRIES AND SPIN”, Prague, July 2013.
[8] FAIR/PANDA Collaboration, Technical Design Report - Muon System, September 2012.
[9] RPC:R. Santonico and R. Cardarelli. Development of resistive plate counters. Nucl. Instr. and Meth., 187:377--380, 1981; R. Santonico and R. Cardarelli. Progress in resistive plate counters. Nucl. Instr. and Meth., A 263:20--25, 1988; ATLAS muon spectrometer technical design report. CERN LHCC9722, ATLAS TDR 10, CERN, 1997; CMS muon technical design report. CMS TDR 3, CERN/LHCC 9732, 1997.
[10] ZDC:C. Adler et al., NIM A 499, 433 (2002); NA49, H. Appelshauser et al., Eur. Phys. J. A 2, 383 (1998).

8.6. References for Section 6.

[1] И. В. Андреев, Хромодинамика и жесткие процессы при высоких энергиях, М., 1981
[2] A.Sissakian, O.Shevchenko, A.Nagaytsev, and O.Ivanov, Phys.Part.Nucl. 41 (2010) 64-100
[3] A. V. Efremov et al., Phys. Lett. B 612, 233 (2005).
[4] J. C. Collins et al., Phys. Rev. D 73, 014 021 (2006).
[5] D. Boer, Phys. Rev. D 60, 014012 (1999).
[6] S. Falciano et al. (NA10 Collab.), Z. Phys. C. 31, 513 (1986);
M. Guanziroli et al., Z. Phys. C 37, 545 (1988).
[7] J. S. Conway et al., Phys. Rev. D 39, 92 (1989).
[8] V. Barone, A. Drago, and P. G. Ratcliffe, Phys. Rep. 359, 1 (2000); hep-ph/0104283.
[9] M. Anselmino, V. Barone, A. Drago, and N. N. Nikolaev, Phys. Lett. B 594, 97 (2004).

APPENDIX 1.

Table 1: Cross sections of J/ψ production in pp colisions at $\sqrt{s} = 24$ GeV

ISUB	process	cross section, [mb]	Comments
	'colour singlet' approach		
86	$gg \to J/\psi g$	$1.429 \cdot 10^{-6}$	
87	$gg \to \chi_{0c} g \to J/\psi\gamma$	$3.348 \cdot 10^{-6}$	
88	$gg \to \chi_{1c} g \to J/\psi$	$3.954 \cdot 10^{-7}$	
89	$gg \to \chi_{2c} g \to J/\psi$	$2.736 \cdot 10^{-6}$	
106	$gg \to J/\psi\gamma$	$3.894 \cdot 10^{-8}$	
	'colour octet' mechanism		
421	$gg \to c\bar{c}[^3S_1^{(1)}]g$	$1.653 \cdot 10^{-6}$	
422	$gg \to c\bar{c}[^3S_1^{(8)}]g$	$5.762 \cdot 10^{-7}$	
423	$gg \to c\bar{c}[^1S_0^{(8)}]g$	$1.742 \cdot 10^{-6}$	
424	$gg \to c\bar{c}[^3P_J^{(8)}]g$	$3.609 \cdot 10^{-6}$	
425	$gq \to qc\bar{c}[^3S_1^{(8)}]$	$1.510 \cdot 10^{-6}$	
426	$gq \to qc\bar{c}[^1S_0^{(8)}]$	$1.817 \cdot 10^{-6}$	
427	$gq \to qc\bar{c}[^3P_J^{(8)}]$	$4.154 \cdot 10^{-6}$	
428	$q\bar{q} \to gc\bar{c}[^3S_1^{(8)}]$	$2.686 \cdot 10^{-7}$	
429	$q\bar{q} \to gc\bar{c}[^1S_0^{(8)}]$	$1.072 \cdot 10^{-8}$	
430	$q\bar{q} \to gc\bar{c}[^3P_J^{(8)}]$	$7.200 \cdot 10^{-8}$	
431	$gg \to c\bar{c}[^3P_0^{(1)}]$	$1.948 \cdot 10^{-5}$	χ_{0c}
432	$gg \to c\bar{c}[^3P_1^{(1)}]$	$2.300 \cdot 10^{-6}$	χ_{1c}
433	$gg \to c\bar{c}[^3P_2^{(1)}]$	$1.592 \cdot 10^{-5}$	χ_{2c}
434	$g\bar{q} \to qc\bar{c}[^3P_0^{(1)}]$	$1.844 \cdot 10^{-5}$	χ_{0c}
435	$g\bar{q} \to qc\bar{c}[^3P_1^{(1)}]$	$4.802 \cdot 10^{-6}$	χ_{1c}
436	$g\bar{q} \to qc\bar{c}[^3P_2^{(1)}]$	$1.836 \cdot 10^{-5}$	χ_{2c}
437	$q\bar{q} \to gc\bar{c}[^3P_0^{(1)}]$	$8.471 \cdot 10^{-9}$	χ_{0c}
438	$q\bar{q} \to gc\bar{c}[^3P_1^{(1)}]$	$4.703 \cdot 10^{-7}$	χ_{1c}
439	$q\bar{q} \to gc\bar{c}[^3P_2^{(1)}]$	$3.571 \cdot 10^{-7}$	χ_{2c}